Article

Neuron

The Cholinergic Basal Forebrain Links Auditory Stimuli with Delayed Reinforcement to Support Learning

Graphical Abstract

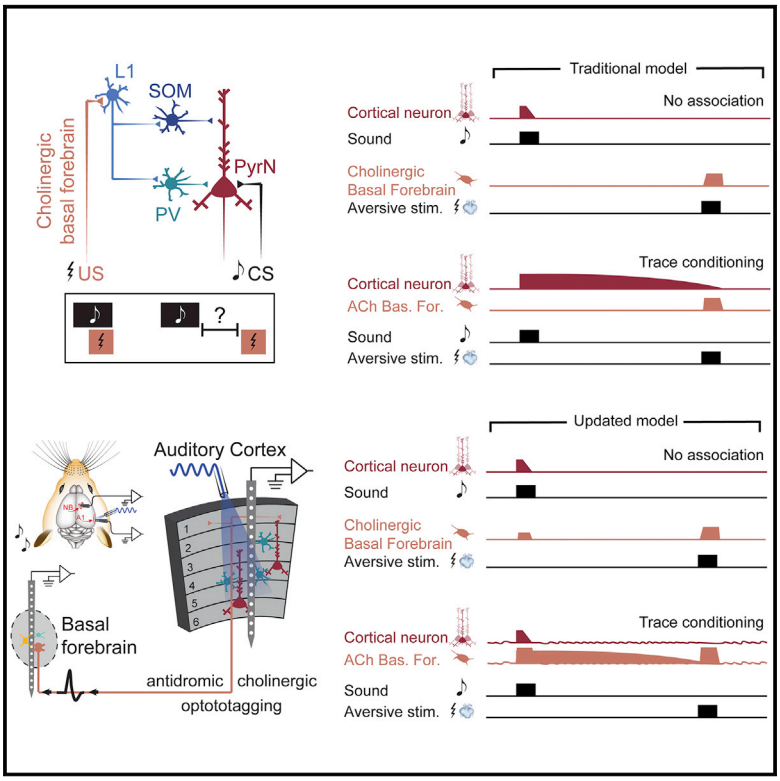

Highlights

- Mice learn to fear sounds that precede aversive reinforcement by a 5-s silent gap
- Auditory cortex neurons rapidly reorganize, but activity does not bridge the 5-s gap
- Optotagged cholinergic basal forebrain neurons encode sound and aversive stimuli
- Basal forebrain neurons bypass the 5-s gap to coordinate auditory cortex plasticity

Authors

Wei Guo, Blaise Robert, Daniel B. Polley

Correspondence

daniel.polley@meei.harvard.edu

In Brief

Sensory stimuli and behavioral reinforcement can be separated by long silent intervals. Guo et al. characterize a distributed neural circuit in the mouse forebrain that supports auditory fear learning by linking brief sounds with aversive events that occur many seconds later.

Guo et al., 2019, Neuron *103*, 1164–1177
September 25, 2019
https://doi.org/10.1016/j.neuron.2019.06.024

CellPress

CellPress

Neuron
Article

The Cholinergic Basal Forebrain Links Auditory Stimuli with Delayed Reinforcement to Support Learning

Wei Guo,[1,3] Blaise Robert,[1] and Daniel B. Polley[1,2,4,*]
[1]Eaton-Peabody Laboratories, Massachusetts Eye and Ear Infirmary, Boston, MA 02114, USA
[2]Department of Otolaryngology, Harvard Medical School, Boston, MA 02114, USA
[3]Present address: Department of Brain and Cognitive Sciences, Picower Institute for Learning and Memory, Massachusetts Institute of Technology, Cambridge, MA 02139, USA
[4]Lead Contact
*Correspondence: daniel.polley@meei.harvard.edu
https://doi.org/10.1016/j.neuron.2019.06.024

SUMMARY

Animals learn to fear conditioned sound stimuli (CSs) that accompany aversive unconditioned stimuli (USs). Auditory cortex (ACx) circuits reorganize to support auditory fear learning when CS-evoked activity temporally overlaps with US-evoked acetylcholine release from the basal forebrain. Here we describe robust fear learning and acetylcholine-dependent ACx plasticity even when the US is delayed by several seconds following CS offset. A 5-s CS-US gap was not bridged by persistent CS-evoked spiking throughout the trace period. Instead, within minutes following the start of conditioning, optogenetically identified basal forebrain neurons that encode the aversive US scaled up responses to the CS and increased functional coupling with the ACx. Over several days of conditioning, bulk imaging of cholinergic basal forebrain neurons revealed sustained sound-evoked activity that filled in the 5-s silent gap preceding the US. These findings identify a plasticity in the basal forebrain that supports learned associations between sensory stimuli and delayed reinforcement.

INTRODUCTION

Animals rapidly learn to fear a neutral sound stimulus (conditioned stimulus [CS]) that overlaps in time with an aversive stimulus (unconditioned stimulus [US]). Auditory fear learning reflects a plasticity at sites of CS and US convergence, including the lateral amygdala, medial division of the medial geniculate body, and auditory cortex (ACx) (Janak and Tye, 2015; Letzkus et al., 2015; McGann, 2015; Weinberger, 2011). Aversive stimuli trigger the phasic release of acetylcholine (ACh) in the ACx via projections from the basal forebrain, which act through local inhibitory microcircuits to modulate the excitability of cortical pyramidal neurons (Froemke et al., 2007; Kuchibhotla et al., 2017; Letzkus et al., 2011; Nelson and Mooney, 2016; Takesian et al., 2018; Urban-Ciecko et al., 2018). During brief windows of disinhibition, the afferent CS trace elicits enhanced spiking of cortical pyramidal neurons (Froemke et al., 2007; Letzkus et al., 2011, 2015; Pi et al., 2013) and induces a persistent and selective potentiation of the CS frequency that can be indexed through increased excitatory synaptic strength (Froemke et al., 2007, 2013), increased spiking (Bakin and Weinberger, 1990, 1996; Blake et al., 2006; Froemke et al., 2013; Ma and Suga, 2003; Quirk et al., 1997), over-representation of the CS frequency in ACx tonotopic maps of sound frequency (Kilgard and Merzenich, 1998), and enhanced perceptual awareness of the CS sound (Aizenberg et al., 2015; Froemke et al., 2013; Reed et al., 2011). Thus, many lines of converging research support a phasic ACh release model as a necessary and sufficient condition for ACx receptive field plasticity related to auditory fear learning, in which selective enhancement of the CS frequency requires a temporal handshake between bottom-up CS-evoked sensory activity and US-evoked ACh release.

One potential challenge to the phasic ACh release model for ACx receptive field plasticity is that it has only been extensively tested with protocols where the CS and US overlap in time. In the real world, robust sensory learning occurs even with delayed behavioral reinforcement. This has been studied in the laboratory with trace conditioning protocols in which the CS is separated from the US by a silent gap ranging from milliseconds to hours (Garcia et al., 1966; Pavlov, 1932; Raybuck and Lattal, 2014). Models of trace conditioning posit that temporal overlap between a CS and delayed US is achieved by extending the CS-evoked response in time until the US arrives (Raybuck and Lattal, 2014). Signatures of persistent auditory CS-induced activity have not been characterized in the ACx but, instead, have been predominantly identified in the hippocampus (Chowdhury et al., 2005), prefrontal cortex (Gilmartin and McEchron, 2005; Siegel et al., 2012), anterior cingulate cortex (Han et al., 2003), medial subdivision of the medial geniculate body (Hoffmann et al., 2018; Plakke et al., 2009), and amygdala (Bauer et al., 2007; Taub et al., 2018a, 2018b). This raises the possibility that the phasic release model for ACx plasticity that supports auditory

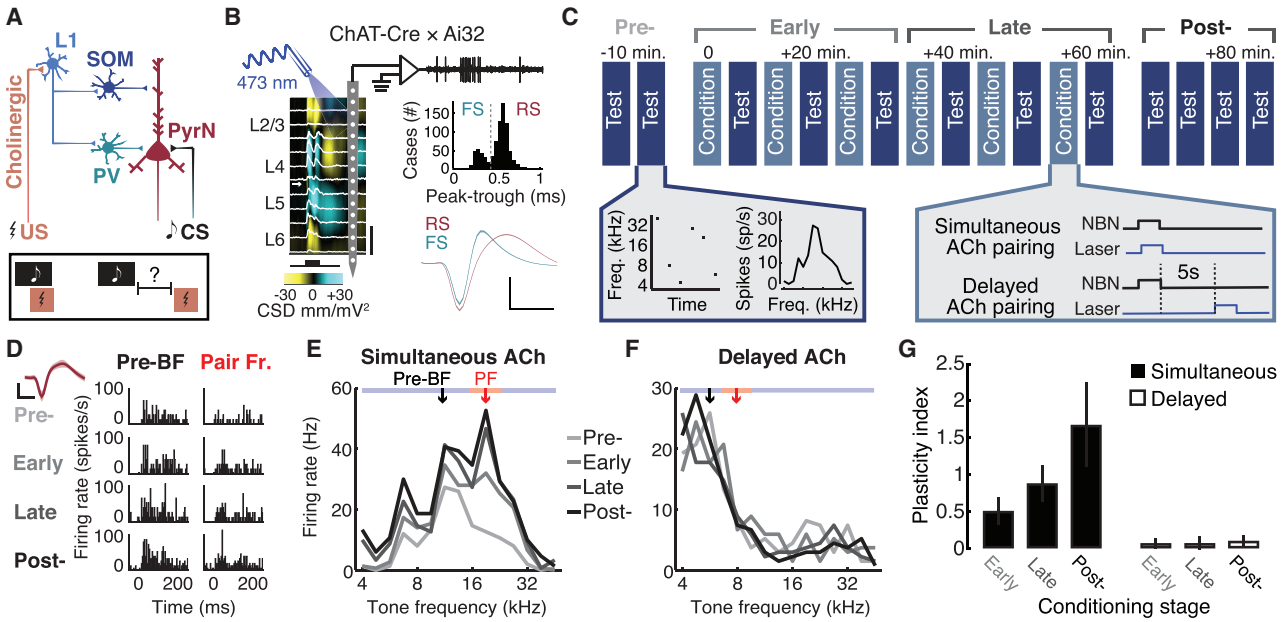

Figure 1. Cholinergic Terminal Activation in the Auditory Cortex Induces Associative Receptive Field Plasticity, but Only When Temporally Overlapping with the CS

(A) Cartoon of ACx circuitry for plasticity and learning when auditory conditioned stimuli (CSs) are paired with aversive unconditioned stimuli (USs). L1, layer 1; SOM, somatostatin; PV, parvalbumin.

(B) Schematic of the strategy to induce ACx receptive field plasticity with local optogenetic activation of cholinergic terminals in ChAT-Cre × Ai32 mice. Extracellular recordings are made from all layers of the mouse A1 during conditioning. Sound-evoked electrophysiological responses are filtered offline to separately analyze unit spiking (white trace), the local field potential (LFP), and the current source density (CSD). The white arrow in the CSD trace identifies the early current sink in L4. Single units isolated from the multiunit recordings were classified as fast-spiking units (FSUs, peak-to-trough delay < 0.4 ms) or regular spiking units (RSUs, peak-to-trough delay > 0.4 ms). Scale bars, 40 μV and 0.5 ms. Spike waveforms reflect the mean of all FSU and RSU amplitudes ± SEM.

(C) Optogenetic pairing and testing protocol for awake head-fixed ACx recording experiments. NBN, narrow-band noise.

(D) Spike PSTHs from a regular spiking unit at the pre-pairing best frequency (BF) and the frequency paired with cholinergic terminal activation (Pair Fr. or PF). Inset: single-unit spike waveform, where shading indicates SEM. Scale bars, 50 μV and 0.4 ms.

(E) Frequency response functions for the same RS unit across conditioning stages. The fold change in normalized spike rate at frequencies far away from the PF (> ± 0.25 octaves, blue) is subtracted from frequencies near the PF (≤ ± 0.25 octaves, red) to compute the plasticity index, where values greater than 0 indicate enhanced firing rates near the paired frequency.

(F) Frequency response functions from an example unit where a 5-s delay separated the offset of sound stimuli and cholinergic axon stimulation.

(G) Mean ± SEM plasticity index across conditioning stages (n = 57/34 units from N = 12/11 mice for simultaneous/delayed ACh pairing).

Data from each individual RS and FS unit are provided in Figure S1.

fear learning only applies to the narrow condition where sound and aversive stimuli overlap in time.

Here we demonstrate that conditioning mice with an auditory CS and a delayed aversive US induces a robust, rapid, and selective plasticity in the primary auditory cortex (A1) that is blocked by local cholinergic antagonists. Temporal alignment of CS and US inputs was not achieved by extending the CS-evoked response throughout the 5-s trace period until the US arrived. Instead, we identify a plasticity within the cholinergic basal forebrain itself that coordinated the temporal alignment of the CS and delayed US by scaling up CS+-evoked responses during the sensory and trace periods. Rather than acting strictly as a gating signal that promotes reorganization of cortical circuits, our findings identify a surprising malleability in the timing and response amplitude of the cholinergic basal forebrain input to the sensory cortex that may support learned associations between sounds and delayed consequences.

RESULTS

Selective Enhancement of Sound Frequencies Paired with Optogenetic Release of ACh

Local circuit plasticity in the ACx that supports auditory fear learning arises from the temporal convergence of a bottom-up sensory trace evoked by the CS and a ACh surge from the basal forebrain evoked by the US (Figure 1A; Bakin and Weinberger, 1996; Froemke et al., 2007; Letzkus et al., 2011). To test the prediction that phasic ACh release from basal forebrain neurons is sufficient to enhance ACx spiking responses to co-occurring sound frequencies, we optogenetically activated cholinergic basal forebrain neurons that project to the ACx by pulsing blue light on the ACx surface of awake, head-fixed ChAT-Cre × Ai32 mice that express channelrhodopsin2 in cholinergic neurons. Extracellular recordings of regular spiking (RS) and fast spiking (FS) units were made from

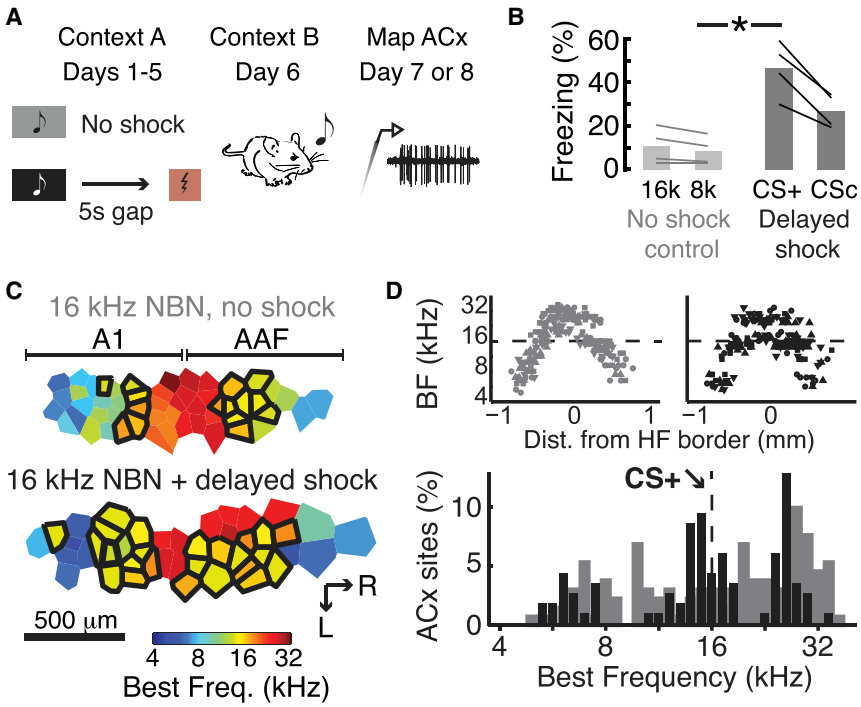

Figure 2. Associative Fear Learning and ACx Map Reorganization Develop Despite a 5-s Silent Gap Separating the CS and US

(A) Mice were assigned to delayed shock (N = 4) or no shock control groups (N = 4) and underwent 5 days of conditioning with interleaved 8- and 16-kHz tones. Freezing behavior was measured on day 6. Tonotopic BF maps from the right auditory cortex (ACx) were delineated on day 7 or 8.

(B) Conditioned freezing behavior to a CS+ tone is observed when a 5-s delay separates the CS and US. The asterisk indicates a significant group × frequency interaction term. Bar plots show mean, lines represent individual mice.

(C) Tonotopic BF maps were reconstructed from microelectrode recordings of multiunit tonal receptive fields from the primary auditory cortex (A1) and anterior auditory field (AAF) (control, n = 118/4; delayed shock conditioning, n = 130/4 [recordings sites/mice]) of the mice behaviorally characterized in (B).

(D) Distortions in the caudal-to-rostral BF mirror reversal gradient (top) over-represent the 16-kHz CS+ frequency, as shown in histograms of BF distributions in tone + delayed shock (black) mice compared with no-shock control mice (gray). Symbols represent data points from different individual mice.

the A1 of awake, head-fixed mice with multi-channel silicon probes (Figure 1B). Single-unit recordings were held for approximately 80 min, during which time auditory receptive fields were characterized with tone pips of varying frequency (test blocks) interspersed with six sound and laser conditioning blocks comprised of 10 pairing trials each (Figure 1C). In support of the phasic ACh release model, pairing narrow-band noise (NBN) bursts with simultaneous optogenetic activation of cholinergic neurons rapidly enhanced spiking of RS units at the paired frequency (n = 57 units, ANOVA main effect for conditioning stage $F = 9.74$, $p < 0.005$, one-sample t tests against a population mean of zero, $p < 0.025$ for all conditioning stages; Figures 1D, 1E, and 1G). Rapid enhancement of spiking at the paired frequency was not observed for FS units, perhaps reflecting earlier observations that A1 inhibitory frequency-receptive fields are slower to reorganize with basal forebrain pairing protocols (Froemke et al., 2007). Plasticity index values for all individual RS and FS units are reported in Figure S1.

A second prediction of the phasic ACh model is that receptive field plasticity would fail to occur when the cholinergic surge arrives after a long delay following the offset of auditory stimulation. We tested this by repeating the same experiment, only with a 5-s delay separating the offset of the NBN burst and the laser onset. In contrast to the receptive field plasticity observed with simultaneous presentation of sound and cholinergic basal forebrain activation, we did not observe selective enhancement of the paired frequency when a 5-s gap separated sound offset and the laser onset (n = 34 RS units, ANOVA main effect for conditioning stage $F = 0.58$, $p = 0.44$, one-sample t tests against a population mean of zero, $p > 0.07$ for all conditioning stages; Figures 1F and 1G).

Fear Learning and ACx Map Reorganization Accompany Extended Auditory Trace Conditioning

Electrophysiological representations of sounds fade away within a few hundred milliseconds following offset. Presumably, A1 receptive fields did not reorganize when the NBN and laser stimuli were separated by a 5-s silent gap because the cholinergic surge arrived in the ACx long after the sensory trace had expired (Metherate and Ashe, 1991). However, behaviorally, associative trace learning can occur when the US begins several seconds, minutes, or even hours after the CS ends (Davis et al., 1989; Garcia et al., 1966; Pavlov, 1932; Raybuck and Lattal, 2014). To determine whether behavioral indications of auditory fear learning could form in spite of a 5-s gap separating the CS and US, we conditioned mice over five consecutive days either with a 16-kHz NBN CS+ followed 5 s later by a foot shock (N= 4) or a no-shock control condition (N = 4) (Figure 2A). On day 6, both groups of mice were introduced to a novel sensory context and presented with interleaved trials of the CS+ frequency or a CS- control (CSc) frequency that was never paired with shock. We found that mice conditioned with a 5-s gap between the CS and US exhibited auditory fear learning that appeared to be virtually identical to previous descriptions with temporally overlapping sounds and foot shocks (Letzkus et al., 2011) (ANOVA group × frequency interaction, $F = 32.3$, $p < 0.0001$; Figure 2B).

These findings demonstrate that auditory fear learning was robust to a 5-s silent gap separating the CS and US even though activating cholinergic axons 5 s after sound offset did not induce A1 receptive field reorganization. There are many possible reasons for this discrepancy. The most straightforward explanation is that ACx receptive field reorganization may not occur when the CS and US are separated by longer temporal gaps. Instead, the critical locus of plasticity could shift to other brain areas, such as

the amygdala, entorhinal cortex, or prefrontal cortex (Raybuck and Lattal, 2014). We addressed this possibility by quantifying tonotopic maps of best frequency (BF) from multiunit recordings in the A1 and the anterior auditory field (AAF) from the same eight mice that underwent behavioral testing (Figure 2C). We found that tonotopic receptive field maps were distorted in mice conditioned with a 5-s CS-US delay (n = 130 recording sites) so that the 16-kHz CS+ frequency was over-represented at the expense of neighboring frequencies compared with the smooth BF gradients measured in no-shock control mice that heard the same sounds without the US (n = 118 recording sites, two-sample Kolmogorov-Smirnov test, $p = 0.02$; Figure 2D).

Rapidly Enhanced Cortical Responses to Sounds Associated with Delayed Reinforcement

These findings demonstrate that auditory fear learning and associative ACx plasticity can occur with several days of auditory trace conditioning but leaves open the question of why A1 receptive field reorganization did not occur when cortical ACh neurons were optogenetically activated 5 s after sound offset. One explanation is that cortical changes linked to trace learning might take days to consolidate and would not be expected to develop over the short timescale of a single conditioning session. To test this idea, we returned to the awake head-fixed single-unit recording preparation. Mice either underwent CS+ conditioning (NBN followed 5 s later by an air puff to the face) or CSc conditioning, where NBN bursts were presented without air puffs. Mice could walk freely on a rotating disk, providing us with the means to measure NBN-elicited freezing during conditioning blocks under head fixation (Figure 3A).

We found that cortical plasticity and auditory learning emerged shortly after the start of conditioning, despite the 5-s gap between the CS and US. NBN-triggered freezing behavior was significantly increased with CS+ conditioning compared with either CSc or a second control, in which air puffs were presented at the 5-s delay but directed away from the face (ANOVA, main effect for group, $F = 6.51$, $p < 0.005$; pairwise comparisons, $p < 0.05$ and 0.01, respectively; Figure 3B). An example A1 RS unit exhibited a rapid and selective increase in firing rate near the CS+ frequency that was not observed in units recorded during a CSc session (Figures 3C and 3D). CS+-specific increases in spiking grew steadily during the early and late stages of conditioning and remained elevated after conditioning ended (CS+ conditioning, ANOVA, $F = 8.98$, $p < 0.005$; Figure 3E). CS-specific receptive field plasticity was significantly greater in CS+ conditioning than CSc conditioning (n = 37/71 for CS+/CSc, Kruskal-Wallis post hoc pairwise comparison, $p = 0.02$; Figure 3E). Forcing air through a narrow aperture creates an audible sound, making any air puff strong enough to be aversive a compound CS-US. However, neither conditioned freezing (Figure 3B) nor A1 receptive field plasticity was observed when the air puff was comparably loud but directed just away from the face, confirming that auditory learning and plasticity reflected the aversive sensation of the air puff, not the sound (n = 26, one-way ANOVA, $F = 2.33$, $p = 0.36$; Figure 3E). Data from individual RS and FS units are provided in Figure S2.

We next pursued two explanations for why A1 receptive fields could be rapidly remodeled with a 5-s delay between NBN and an air puff (Figure 3E) but not with a 5-s delay between NBN and optogenetic release of ACh (Figure 1G). The first possibility was that pairing sound with delayed air puffs might have induced a prolonged representation of CS+ sound so that it persisted throughout the 5-s silent interval until the US-evoked ACh surge arrived (Figure 3F). We examined the change in spike rate in RS units, FS units, and unsorted multiunit clusters. We also measured the power in the local field potential (LFP) and current source density (CSD) when filtered at frequencies ranging from theta (4–8 Hz) to high gamma (50–120 Hz). We could not identify any electrical signature of the CS+ that persisted more than a few hundred milliseconds after sound offset. The response amplitudes of all signals measured just prior to the onset of the air puff were comparable with baseline levels prior to CS+ onset, ruling out the possibility that A1 neurons bridged the extended CS-US gap by prolonging the CS+ representation until the US arrived (Figure 3G).

Cholinergic Antagonists Block Rapid ACx Receptive Field Remodeling with Delayed Reinforcement

A second possibility was that A1 reorganization with CS-US trace conditioning protocols might not require cholinergic inputs in the ACx. To test this explanation, we injected a drug cocktail containing both muscarinic and nicotinic receptor antagonists into the A1 approximately 30 min prior to the start of recordings from awake, head-fixed mice from the same location (Figure 4A). To confirm the efficacy of the drug, we optogenetically activated cholinergic axons in the A1 and measured a robust cholinergic potential in the layer 2/3 (L2/3) CSD of ChAT-Cre × Ai32 mice with no injections or with vehicle injections (Figure 4B). Laser-evoked cholinergic potentials were virtually eliminated after cholinergic antagonists, down to the level observed in wild-type mice that do not express ChR2 (unpaired t tests; drug versus wild-type, $p = 0.45$; drug versus vehicle, $p = 0.006$; drug versus un-injected ChAT, $p = 0.0001$; Figure 4C).

We next tested whether cholinergic receptor antagonists would block A1 receptive field plasticity induced by auditory trace conditioning (Figure 4D). Tuning functions and peri-stimulus time histograms (PSTHs) from example units demonstrate the expected enhancement of the CS+ frequency after vehicle injection but no change in A1 tuning when cholinergic synapses are blocked (Figures 4E–4G). Blocking cholinergic receptors in the ACx prevented receptive field reorganization at all time points (one-sample t tests against a population mean of 0; $p > 0.67$ for early, late, and post-conditioning stages), in contrast to the rapid and specific reorganization observed after local injections of vehicle solution (n = 24/25 RS units for drug/vehicle, Kruskal-Wallis test, $p = 0.003$; Figure 4H). Data from individual RS and FS units are provided in Figure S3.

Recording from Cholinergic Basal Forebrain Neurons that Project to the ACx

These findings were puzzling. On the one hand, we observed selective and persistent enhanced spiking evoked by sound frequencies paired with simultaneous cholinergic terminal activation, but not when ACh terminal activation lagged sound offset by 5 s (Figure 1G). On the other hand, using an air puff US instead of the laser pulse induced receptive field reorganization that

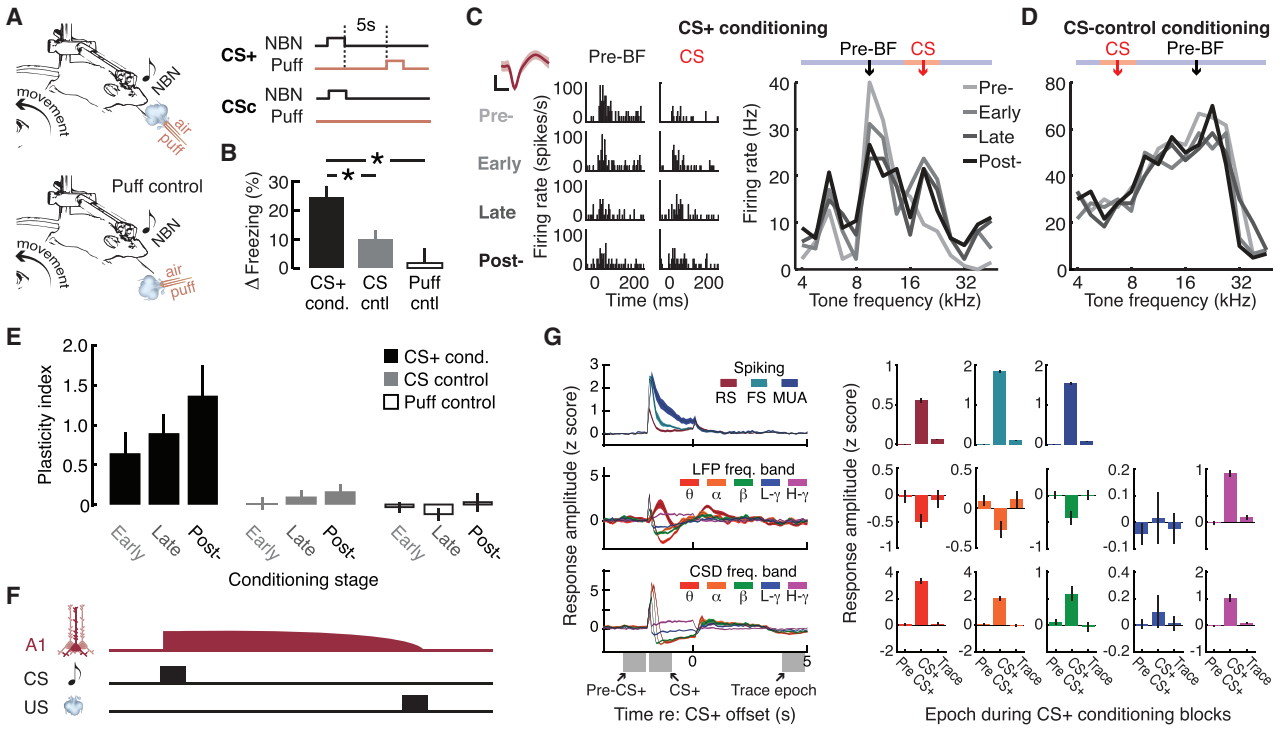

Figure 3. Rapid Emergence of A1 Receptive Field Plasticity and Associative Learning Despite a Long Delay Separating the CS and Aversive Reinforcement

(A) Preparation to study the emergence of plasticity and conditioned freezing in head-fixed mice.

(B) Freezing behavior on the rotary treadmill. Asterisks indicate significantly increased freezing to the CS sound during CS+ conditioning, in which a 5-s silent gap separated the offset of NBN and the onset of the air puff US (n = 16 sessions) compared with CS control (cntl) conditioning, where NBN is presented without air puffs (n = 18 sessions), or an additional control group, where NBN precedes air puffs that are aimed away from the face (n = 5 sessions). Bar plots show mean ± SEM. Asterisks indicate $p < 0.05$ with post hoc pairwise comparisons.

(C) Left: tone-evoked PSTH from a representative regular spiking unit across conditioning stages. Scale bars, 20 μV and 0.4 ms. Right: frequency receptive field from the same unit across conditioning stages. The fold change in normalized spike rate for frequencies far from the CS (blue) is subtracted from that at or near the CS+ (red) to compute the plasticity index, where values greater than 0 denote CS-specific frequency enhancement.

(D) No changes in a frequency receptive field from a representative RS unit recorded in a CS control session.

(E) Mean ± SEM; plasticity index across conditioning stages (n = 37/71/20 RS units from N = 11/12/3 mice for CS+, CSc, and air puff control conditions). Data from each individual RS and FS unit are provided in Figure S2.

(F) Schematic of persistent ACx activity throughout the trace period in CS+ conditioning.

(G) Peri-stimulus time histograms of electrophysiological measures from CS+ conditioning trials. Top row: multiunit (MUA), fast-spiking (FS) and regular spiking (RS) firing rates. Center row: LFP amplitude filtered across theta (4–8 Hz), alpha (8–12 Hz), beta (12–25 Hz), low-gamma (25–50 Hz), and high-gamma (50–120 Hz) frequency bands. Bottom row: CSD amplitude filtered across a range of frequencies. Data are mean ± SEM. Right: bar plots provide the mean ± SEM amplitude of each neurophysiological signal shown at the left, quantified during a 1-s period immediately before the NBN burst (Pre-CS+), during the NBN burst (CS+), and immediately prior to air puff onset (trace epoch). Bar hue corresponds to the physiological signal shown at the left.

could bridge the 5-s silent gap between the CS and US (Figures 2D and 3A–3E). We found no evidence of a persistent CS trace in the A1 that would sustain the acoustic representation until the US arrived (Figures 3F and 3G), but the receptive field reorganization was blocked by local injection of cholinergic antagonists (Figure 4). This led us to question the assumption that cholinergic inputs from the basal forebrain were only elicited by the US. If, instead, cholinergic basal forebrain inputs were activated by the CS as well as the US during learning, then the cholinergic input would functionally bypass the 5-s gap and temporally coincide with the afferent sensory trace to establish the CS-US temporal handshake.

To test this hypothesis, we recorded from optogenetically identified cholinergic basal forebrain neurons that project to the ACx (ChACx). To identify the highest density of ChACx neurons, we first performed an anatomy experiment in which fluorescent red retrobeads were injected into the A1 of ChAT-Cre × Ai32 mice (N = 4) (Figures 5A and 5B; Figure S4). We identified enhanced yellow fluorescent protein (EYFP)+ cholinergic neurons throughout the rostral-caudal extent of the basal forebrain (Figure 5C, top). Bead+ neurons clustered in two locations: (1) a rostral-ventral-medial region that overlaps with the nuclei of the diagonal band and rostral *substantia innominata* and (2) a more dorsal-lateral zone at the extreme caudal tail of the basal forebrain bordering the *globus pallidus*, an area that is sometimes referred to as the *nucleus basalis* (Figure 5C, center). The highest density of ChACx cells was found in this latter region, at the extreme caudal tail of the basal forebrain (Figure 5C,

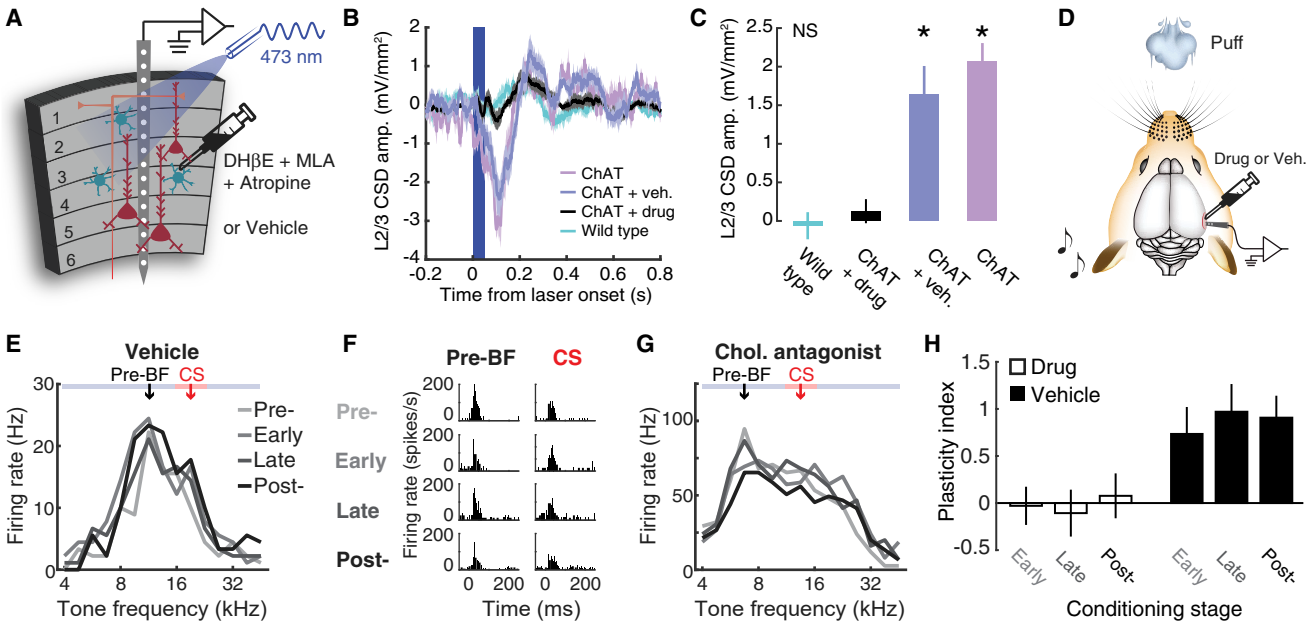

Figure 4. Cholinergic Receptor Antagonists Block Cortical Receptive Field Plasticity that Emerges during Trace Conditioning

(A) A small volume of solution containing cholinergic receptor antagonists or a vehicle control was injected into the A1 approximately 30 min prior to awake recordings (N = 5 mice).

(B) A brief pulse of blue light elicits a cholinergic potential in the L2/3 CSD amplitude of ChAT-Cre × Ai32 mice with or without vehicle injection but not after injection of antagonists or in wild-type mice. Data represent mean ± SEM.

(C) Peak amplitude of the layer 2/3 CSD following laser onset. Data represent mean ± SEM. Asterisks indicate $p < 0.01$ with an unpaired t test relative to the ChAT + drug group after correcting for multiple comparisons. NS, not significant.

(D) Single-unit recordings were made from the A1 during CS+ conditioning in 4 of 5 mice (n = 24/25 regular spiking units for drug/vehicle).

(E) Frequency response functions from an example unit recorded after vehicle injection. The fold change in normalized spike rate for frequencies far from the CS (blue) is subtracted from that at or near the conditioned stimulus (red) to compute the plasticity index, where values greater than 0 denote CS-specific frequency enhancement.

(F) Tone-evoked PSTHs after injection of cholinergic antagonists from a representative regular spiking unit.

(G) Frequency receptive field from the same unit across conditioning stages.

(H) Mean ± SEM; plasticity index across conditioning stages.

Data from each individual RS and FS unit are provided in Figure S3.

bottom; Kim et al., 2016), although, even in the highest-density section, the majority of ChAT+ neurons (~73%) did not contain retrobeads. The sparse projection underscored the need for an approach that could functionally isolate basal forebrain → ACx cholinergic projection neurons from other neighboring ChAT+ neurons that do not project to the ACx. This was accomplished by flashing blue light onto the surface of the ACx to trigger action potentials in cholinergic ACx axons and then recording the antidromic spike near the cell body in the basal forebrain (Figure 5D).

In rare instances where brief (50-ms) optogenetic activation of ACx cholinergic axons activated basal forebrain single units (n = 176 of 1,566 recorded units), we noted that responses fell into two categories: short-latency spikes with low jitter in spike timing (Figure 5E, unit 1) or a longer latency burst of irregularly timed spikes (Figure 5E, unit 2). Either type of unit could have native auditory responses featuring well-defined tonal receptive fields with short-latency sound onset responses (Figure 5F). Among basal forebrain units driven both by laser and pure tones (n = 81), plotting the first spike latency against the first spike latency jitter revealed a sparse set of basal forebrain units (1.2%, n = 20 of 1,566 units) that stood apart from the remaining sample of recordings (Figure 5G). We operationally defined the short-latency, low-jitter population as directly activated ChACx units, whereas the longer-latency irregular spikes presumably arose through synaptic transmission via reafferent or local circuits within the basal forebrain and were therefore classified as not ChACx units (NChACx, n = 61) (Williamson and Polley, 2019; Figure 5H).

Optogenetic activation of cholinergic axon terminals increased the firing rates in basal forebrain units as well as ACx units, although cortical regular spiking unit (RSU) activation (n = 82) was significantly weaker and presumably arose through intracortical disinhibition (Letzkus et al., 2011; Pi et al., 2013; Takesian et al., 2018) or direct photoactivation of the sparse population of ChAT+ and VIP+ cortical interneurons (Eckenstein and Baughman, 1984) (Kruskal-Wallis test; post hoc pairwise comparisons, $p < 1 \times 10^{-6}$; Figure 5I). We confirmed an earlier report that basal forebrain units were driven by aversive reinforcement cues because air puff-evoked spiking was significantly higher in either cell type than in ACx RSUs (Hangya et al., 2015; Harrison et al., 2016; Letzkus et al., 2011; Lin and Nicolelis, 2008) (Kruskal-Wallis test, both pairwise comparisons $p < 1 \times 10^{-6}$; Figure 5J). Importantly, both ChACx and NChACx units in the caudal tail of the

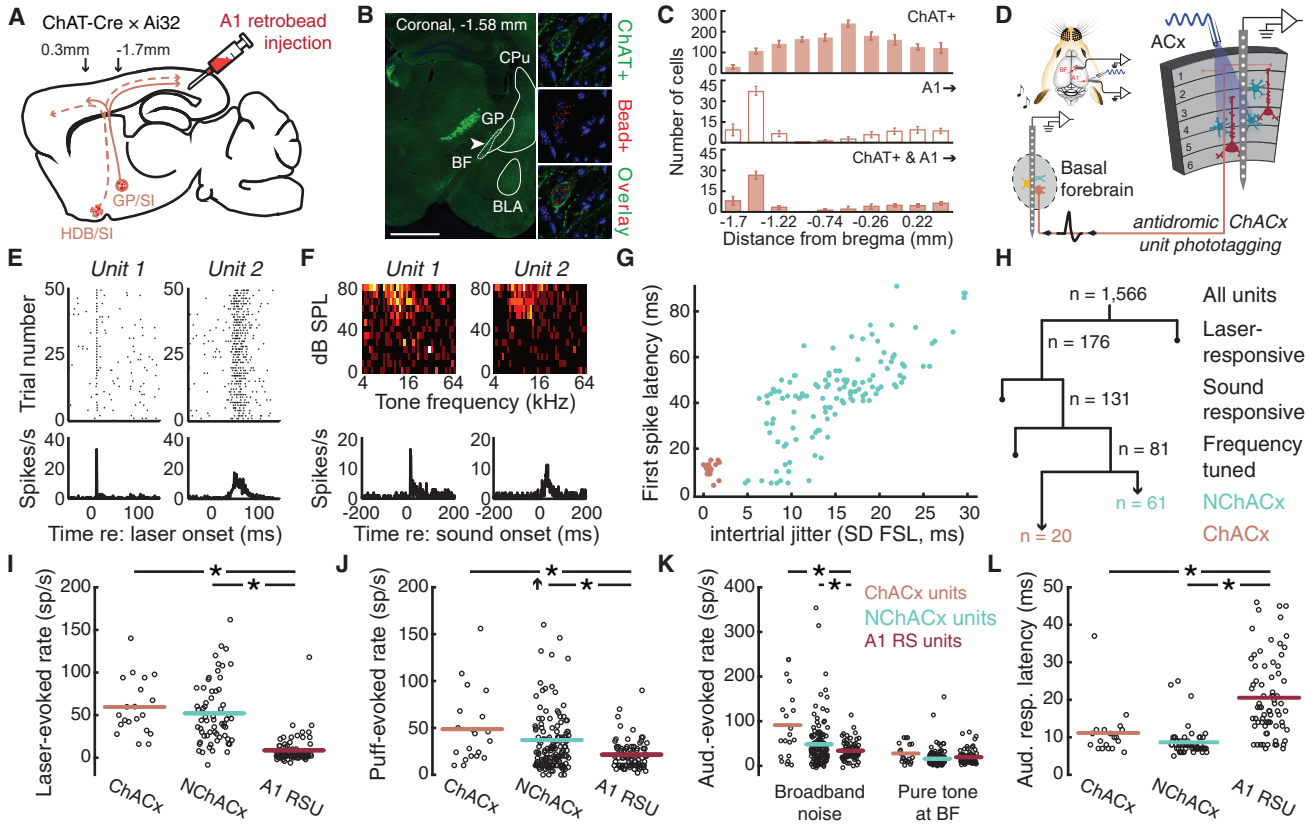

Figure 5. Dual Encoding of Sensory and Reinforcement Signals in the Basal Forebrain

(A) Mid-sagittal mouse brain cartoon showing the strategy for retrograde transport of fluorescent microbeads from the A1 to cholinergic nuclei in the basal forebrain. GP, *globus pallidus*; HDB, horizontal limb of the diagonal band; SI, *substantia innominata*. Arrows depict the zone of anatomical reconstructions expressed relative to the bregma.

(B) Coronal photomicrographs showing EYFP in cholinergic (ChAT+) neurons, retrobeads in ACx projection neurons and the overlay. CPu, caudate putamen; BLA, basolateral amygdala; BF, basal forebrain. Scale bar, 1 mm.

(C) Histograms of ChAT+, bead+, or both ChAT+ and bead+ cells across the caudal-to-rostral extent of the basal forebrain. Additional information regarding bead injection sites is provided in Figure S4.

(D) Strategy for antidromic phototagging of basal forebrain ChAT+ neurons that project to the ACx (ChACx).

(E) Rastergram (top) and PSTH (bottom) of laser-evoked spiking in two basal forebrain units.

(F) Frequency response areas and tone-evoked PSTHs from the same units.

(G) First spike latency (FSL) and FSL jitter evoked by the laser in 81 tone- and laser-responsive basal forebrain units.

(H) Functional categorization of all basal forebrain single unit recordings. Brown coloring, ChACx (n = 20); aqua coloring, indirectly activated neurons operationally defined as not ChACx (NChACx, n = 61).

(I–K) Firing rates evoked by the ACx laser pulse (I), air puff (J), and either broadband noise bursts or BF tones (K, left and right) in ChACx, NChACx and A1 RS units (n = 82). The upward arrow indicates one outlier.

(L) First spike latency in ChACx, NChACx, and A1 RS units evoked by broadband noise bursts. Horizontal lines represent the sample mean; each single unit is represented by a single point. Asterisks indicate significant ($p < 0.05$) post hoc pairwise differences with the Kruskal-Wallis statistic.

basal forebrain exhibited vigorous responses to noise bursts and pure tones before any conditioning had taken place, as suggested by recordings from unidentified cell types in the caudal region of the *globus pallidus* and *nucleus basalis* (Chernyshev and Weinberger, 1998; Maho et al., 1995; Figure 5K). The presence of strong, "native" responses to tones prior to the onset of conditioning may differ from recordings in rostral areas of the basal forebrain. For example, unit recordings from the medial septal complex show vigorous native responses to high-intensity broadband sounds but not to tones (Zhang et al., 2018). Recordings near the nuclei of the diagonal band reveal strong responses to tones, but only after they have been associated with reinforcement (Harrison et al., 2016; Lin and Nicolelis, 2008). Auditory response latencies in the caudal tail of the basal forebrain were shorter than latencies reported in the lateral amygdala (Quirk et al., 1995) and even shorter than ACx RSUs (Figure 5L) and presumably arose from monosynaptic inputs from medial short-latency regions of the auditory thalamus (Chavez and Zaborszky, 2017; Hackett et al., 2011) (11.2 ± 1.51, 8.7 ± 0.47, and 20.5 ± 1.16 ms for ChACx, NChACx, and A1, respectively; Kruskal-Wallis test for the A1 versus the basal forebrain group, $p < 0.02$ for each comparison).

Transiently Enhanced Functional Connectivity between the Basal Forebrain and ACx at the Onset of Auditory Trace Conditioning

These experiments demonstrate that single-unit spike trains in the caudal tail of the basal forebrain encode both sensory and reinforcement cues. The short response latencies in ChACx units would provide sufficient time for cholinergic inputs to engage the disinhibitory microcircuit in the ACx ahead of the arrival of the afferent sensory trace (Letzkus et al., 2011; Pi et al., 2013; Urban-Ciecko et al., 2018). These findings support our hypothesis that ACx circuits could integrate CS and US inputs across a 5-s gap because, in effect, there would not be a 5-s gap separating the arrival of the auditory sensory trace and the transient surge in ACh. However, if basal forebrain → ACx units respond to all sounds, then one might expect ACx receptive fields to reorganize even in response to sounds presented outside of a behavioral context. This was clearly not the case because ACx receptive field plasticity was only observed under conditions where sounds were paired with reinforcement (i.e., CS+ conditioning but not CS-control conditioning) (Figures 2D and 3E).

We reasoned that the influence of ChACx spikes on A1 units must somehow be amplified during CS-US conditioning in a manner not observed when sounds are presented without behaviorally relevant consequences. To this point, we observed that ChACx units rapidly modify their tonal receptive fields to enhance spiking at the CS+ frequency, much like ACx RS units (Figures 6A and 6B). The plasticity index for ChACx units was significantly enhanced early and late in conditioning (Wilcoxon signed-rank tests against a median of 0, $p < 0.005$ for early and late) and was significantly greater for CS+ conditioning than for CSc conditioning ($n = 10/10$ for CS+/CSc early and late conditioning, Kruskal-Wallis test, $p < 0.05$). Unlike ACx receptive field plasticity, ChACx tuning reverted to baseline shortly after conditioning was terminated (post-conditioning, Wilcoxon signed-rank test against a median of 0, $p = 0.07$), suggesting that plasticity within cholinergic projection neurons might be involved in the induction but not maintenance of ACx plasticity (Chubykin et al., 2013). Importantly, enhanced responses to the CS+ frequency were significantly greater in ChACx units than in NChACx units ($n = 10/24$, respectively, unpaired t test, $p < 0.001$; Figure 6B), suggesting that rapid reorganization of sensory tuning in the caudal basal forebrain is cell-type-specific (Maho et al., 1995).

In addition to scaling up spike rates at the CS+ frequency, we also observed a transient increase in the functional connectivity between the basal forebrain and ACx at the initiation of learning. To directly estimate the feedforward influence of basal forebrain unit spikes on the ACx, we measured changes in the amplitude of the CSD from various layers of the A1 that were temporally locked to spikes from individual basal forebrain units (Figure 6C). Because the CS and US directly elicited spiking in both brain areas, we focused on changes in the spike-triggered CSD amplitude during the spontaneous period between trials, when no explicit stimuli were presented (Figure 6D). Unsurprisingly, individual basal forebrain unit spikes were not associated with strong time-locked network activity from the upper layers of the ACx during pre-conditioning baseline recordings. This weak overall influence was maintained throughout CSc conditioning blocks for both basal forebrain cell types (Figure 6E). During CS+ conditioning blocks, however, we noted a striking increase in the strength of the spike-triggered CSD, particularly for ChACx units. In L2/3, the spike-triggered CSD amplitude averaged over the first three CS+ blocks was significantly increased above baseline for both ChACx and NChACX units (one-sample t tests against a population mean of 0; $p < 0.01$ for both), but the change for ChACx units was greater than for NChACx units and greater than the change during CSc conditioning (unpaired t tests, $p < 0.05$ for both comparisons; Figure 6F). Changes in basal forebrain spike-triggered cortical CSD were also noted in deeper layers, where NChACx units showed the strongest changes during CS+ blocks (one-sample t tests against a population mean of 0; $p < 0.0005$ for both early and late conditioning; Figure 6G).

Gamma rhythms in the LFP are well-established signatures of cognitive processing, sensory learning, and inter-regional communication (Buzsáki and Wang, 2012; Fries, 2015; Miltner et al., 1999). We analyzed coherence in the gamma-band LFP (40–80 Hz) from simultaneous recordings in the basal forebrain and ACx during the CS, trace, US, and spontaneous epochs of conditioning trials (Figures 6D and 6H). We found that gamma coherence between the basal forebrain and ACtx was significantly enhanced during the initial blocks of CS+ conditioning compared with CSc blocks. Enhanced gamma coherence was not limited to the CS or trace periods but, rather, was observed throughout the entire trial, even during the inter-trial interval period ($n = 176/198$ samples CS+/CSc, unpaired t tests, $p < 0.005$ for each of the four periods; Figure 6I). Increased gamma coherence during NBN-air puff pairings declined monotonically across the six conditioning blocks for all response epochs within the conditioning trial (one-way ANOVA, $F = 454$, $p < 1 \times 10^{-6}$; Figure 6J). Persistent changes outside of the CS and US periods confirm that elevated gamma coherence is likely not an epiphenomenon of a stimulus-induced increase in gamma power (Buzsáki and Schomburg, 2015; Buzsáki and Wang, 2012) but, instead, might be coordinated by a lower frequency rhythm generated by a common input to both areas, such as the amygdala (Taub et al., 2018a).

Reorganized Sound Processing in the Cholinergic Basal Forebrain with Extended Auditory Trace Conditioning

Basal forebrain recordings during conditioning revealed a transient increase in spike rates to the CS+ frequency (Figure 6B), enhanced spike-triggered network response amplitude in the A1 (Figures 6F and 6G), and increased gamma band coherence with the A1 (Figures 6I and 6J) during CS+ conditioning blocks but not CSc blocks. These data provide a plausible explanation for how sound can evoke responses from basal forebrain units outside of a learning context but only induce cortical plasticity when paired with behavioral reinforcement. However, because enhanced spike-triggered CSD and gamma coherence were observed throughout CS+ conditioning blocks, even during the inter-trial interval, it was not entirely clear that these physiological changes reflected a signature of CS-US associative trace learning. Alternatively, it could have reflected a general state-dependent shift between listening to sounds in a passive context

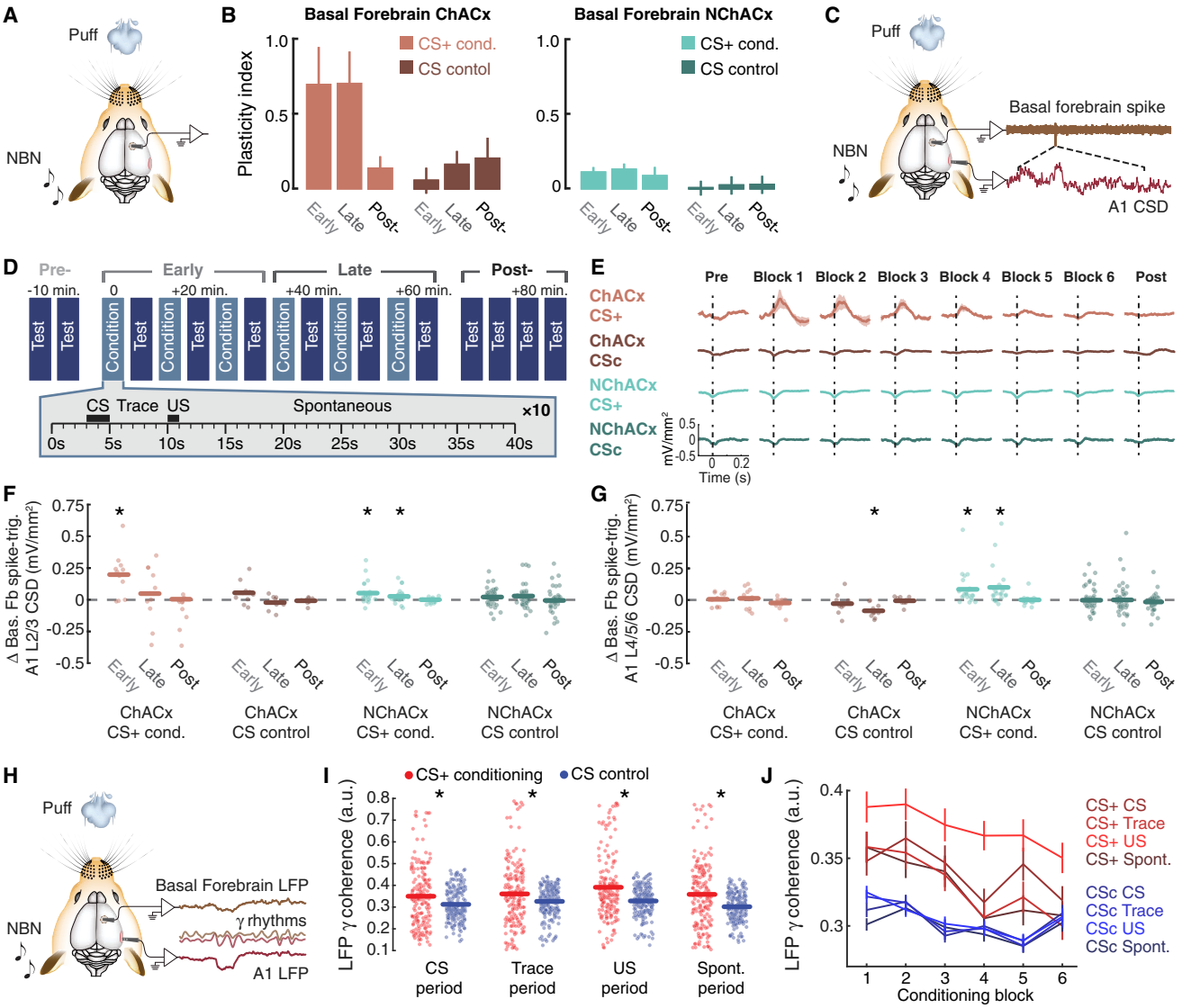

Figure 6. Plasticity and Enhanced Functional Connectivity between the Basal Forebrain and ACx during Auditory Trace Conditioning

(A) Single unit recordings were made from the basal forebrain during trace conditioning with narrowband noise and air puffs.

(B) Plasticity index across conditioning stages for ChACx and NChACx units in CS+ conditioning (lighter hue, n = 10/24 for ChACx/NChACx) and CS control conditioning (darker hue, n = 10/37 for ChACx/NChACx), measured during test blocks. Data from each individual ChACx and NChACx units are provided in Figure S5.

(C) CSD signals in the A1 could be plotted relative to the incidence of individual spikes recorded in basal forebrain units.

(D) Ten conditioning trials were performed in each of six conditioning blocks. Each trial could be broken down into CS, trace, US, and spontaneous epochs.

(E) Mean ± SEM; A1 L2/3 CSD amplitude triggered by spiking in ChACx and NChACx units during the spontaneous epoch in each of six CS+ or CSc conditioning blocks.

(F and G) Change in the spike-triggered CSD recorded from L2/3 (F) or L4/L5/L6 (G) of the A1, expressed relative to the pre-conditioning value. Circles represent data from individual basal forebrain units. Asterisks represent a significant difference from a population mean = 0 (one-sample t test).

(H) LFP signals were recorded simultaneously in the basal forebrain and A1 and filtered in the gamma band (40–80 Hz).

(I) LFP gamma-band coherence between the ACx and basal forebrain, averaged over the first three conditioning blocks during CS, trace, US, and spontaneous trial epochs (176 CS+ and 198 CSc recordings). Asterisks indicate p value < 0.005 with unpaired t tests.

(J) Mean ± SEM gamma coherence for each conditioning block.

(CSc blocks) versus listening to sounds while repeatedly being subjected to aversive air puffs (CS+ blocks). These possibilities could be disambiguated by interleaving CS+ and CSc trials while recording from cholinergic basal forebrain units, but it proved to be impossible to hold single units over these extended duration recordings sessions. Instead, we performed bulk fiber imaging of calcium signals from cholinergic cells in the caudal basal forebrain using transgenic mice that express the genetically

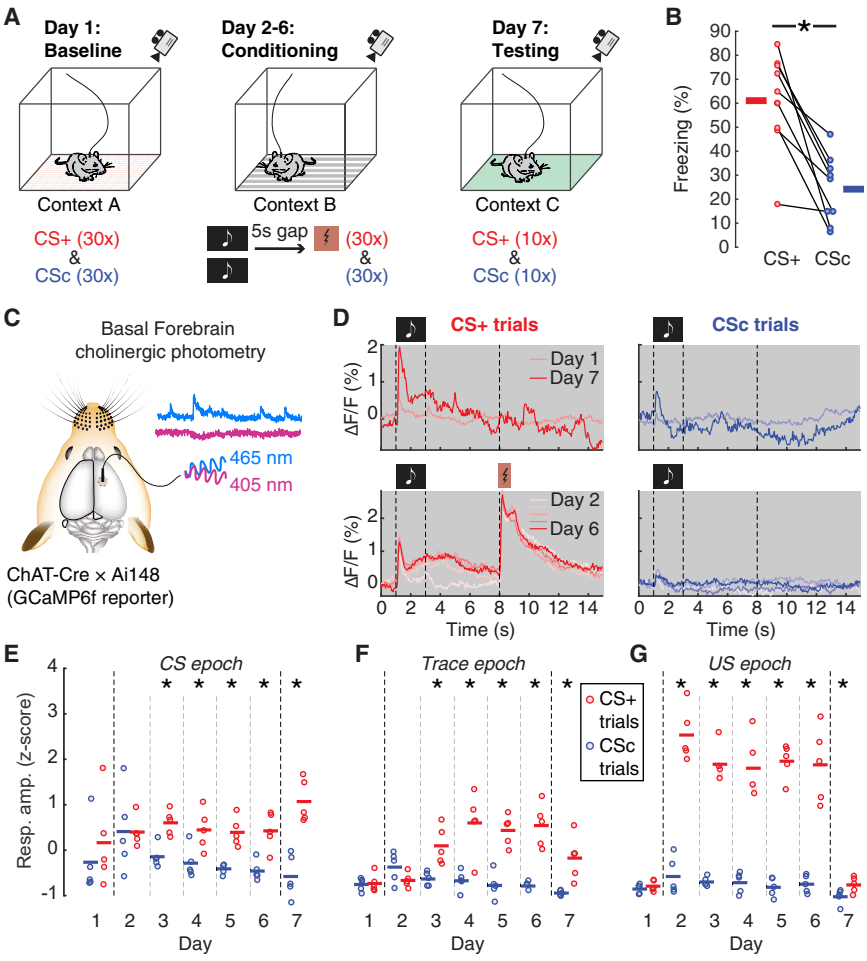

Figure 7. Reorganization of Cholinergic Basal Forebrain Responses with Extended Auditory Trace Conditioning

(A) Protocol for extended trace conditioning with interleaved blocks of CS+ and CSc trials.

(B) Five days of interleaved conditioning with CS+ and CS control tones produced robust auditory trace fear learning when freezing was measured on the testing day. Lines represent individual mice (N = 9). Solid bars represent mean values. *p = 0.004 with Wilcoxon signed-rank test.

(C) Bulk fiber-based calcium imaging from basal forebrain cholinergic neurons was performed in freely moving ChAT-Cre × Ai148 mice. Dual-wavelength imaging allowed subtraction of calcium-independent fluorescence (405 nm) from calcium-dependent fluorescence (465 nm).

(D) Top: fractional change in fluorescence evoked by the CS+ (left) and CSc (right) stimuli during baseline (day 1) and testing (day 7) sessions. Bottom: fractional change in fluorescence evoked by the CS+ and shock (left) and CSc (right) stimuli during the five conditioning days (days 2–6).

(E–G) *Z*-scored response amplitudes measured during CS+ and CSc trials across all 7 days of the training procedure. Response amplitudes are calculated separately for the CS (E), trace (F), and US (G) epochs. Each mouse is represented by a circle. Horizontal lines represent mean values. Asterisks indicate $p < 0.05$ with permutations tests.

encoded calcium indicator GCaMP6f in cholinergic neurons (ChAT-Cre × Ai148).

Fiber photometry recordings were stable over time, allowing us to record from the cholinergic basal forebrain over a 7-day behavioral training procedure with interleaved CS+ and CSc conditioning as opposed to a single 80-min recording session with either CS+ or CSc conditioning. Like the auditory trace fear conditioning described in Figure 2, mice were conditioned over five consecutive days with interleaved blocks of CS+ and CSc NBN bursts before being transferred to a different sensory context for a final test session with randomly interleaved CS+ and CSc trials (Figure 7A). As per our earlier behavioral experiments (Figure 2B), mice exhibited significantly greater freezing to the CS+ frequency than the CSc frequency when studied on the test day (day 7) (Wilcoxon signed-rank test, n = 9, p = 0.004; Figure 7B). Having confirmed stimulus-specific auditory trace learning, we next analyzed changes in sound-evoked activity from cholinergic cells in the caudal basal forebrain, measured during the behavior in the 5 of 9 mice that provided a measurable bulk calcium signal throughout the 7-day recording period (Figure 7C).

We observed that NBN stimuli evoked clear responses from cholinergic neurons on day 1 of baseline testing, confirming our observation of native sound-evoked responses in the caudal basal forebrain (Figures 5K and 7D, day 1). On the final test day, we observed enhanced responses to the CS+ frequency compared with interleaved trials of the CSc frequency (Figure 7D, day 7). Examination of the responses during the five conditioning days revealed a striking increase in CS+-evoked cholinergic activity beginning on day 3 that remained elevated throughout the 5-s trace period separating sound and foot shock (Figure 7D, days 2–6). Responses to interleaved CSc stimuli during conditioning were of lower amplitude and restricted to sound onset. We quantified the fractional change in fluorescence for CS+ and CSc control frequencies over the 7-day period during three epochs within a trial: (1) the CS period (0.5-s duration beginning at sound onset), (2) the trace period (5-s duration beginning at CS offset), and (3) the US period (4-s duration, beginning 5 s after CS offset). This provided 42 unique data points per implanted mouse (N = 5). Because the GCaMP signal-to-noise ratio varied from mouse to mouse, we converted the distribution of these 42 ΔF/F values to *Z* scores for each mouse before making group comparisons. We found that CS+ responses became significantly greater than CSc responses in both the CS and trace periods beginning on the second day of trace conditioning (day 3) and remained elevated throughout the final day of testing (permutation tests, $p < 0.05$ for all; Figures 7E and 7F, respectively). Aversive stimuli, such as air puffs (Figure 5J) or foot shocks (Figure 7G), strongly activated cholinergic basal forebrain neurons (permutation tests, $p < 0.05$ for days 2–6), and activity even remained significantly

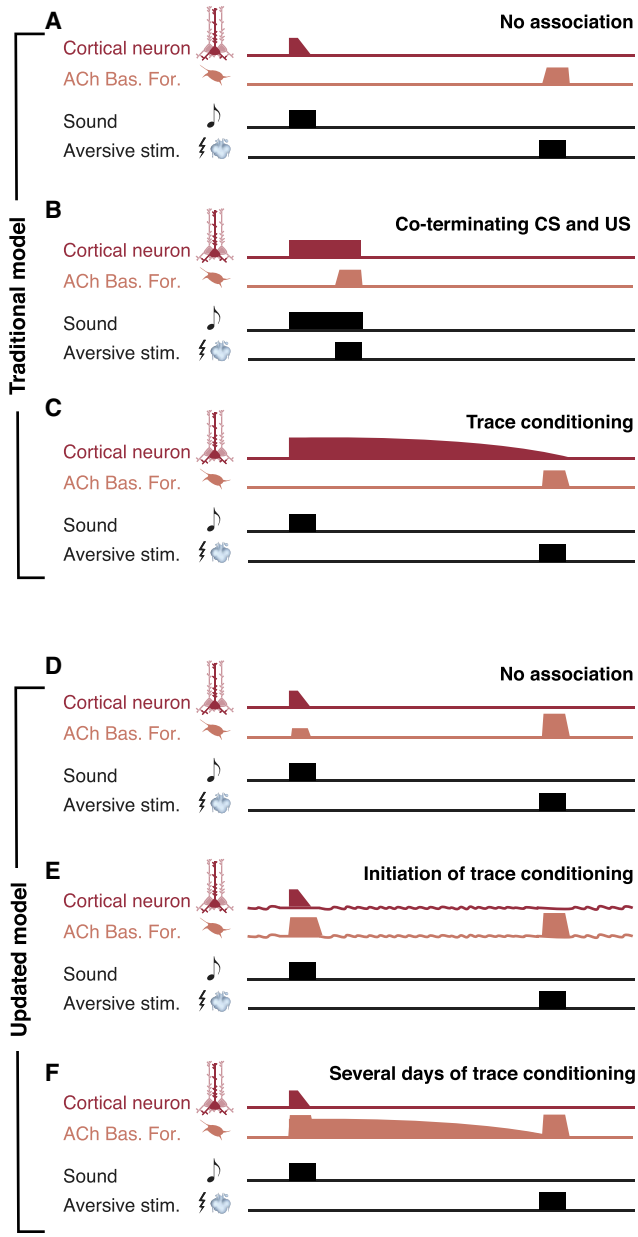

Figure 8. Cartoon Models for Cortical and Basal Forebrain Dynamics that Link Conditioned Stimuli with Delayed Reinforcement

(A–C) Traditional model for encoding unassociated CSs and USs (A), co-terminating CSs and USs (B), and persistent CS-evoked cortical activity with trace conditioning (C).

(D–F) Our findings identify native auditory responses in the basal forebrain and ACx (D) that are rapidly scaled up at the start of trace conditioning (E), allowing basal forebrain neurons to bypass rather than bridge the CS-US temporal gap (F).

elevated during the US period on CS+ trials on day7, when no foot shock was presented (permutation test, $p = 0.03$). Changes in cholinergic response strength across days and recording epochs could not be explained by the movement status of the animals (Figure S6). These data, along with CS+-specific remodeling of ChACx receptive fields (Figure 6B; Figure S5), confirm that sensory plasticity within the cholinergic basal forebrain is stimulus-specific and not solely reflective of generalized state changes.

DISCUSSION

During auditory fear learning, A1 receptive fields are rapidly remodeled to enhance sound frequencies paired with aversive stimuli. Studies of ACx plasticity related to auditory fear learning have primarily used conditioning protocols where the CS and US co-terminate (Figures 8A and 8B). With trace conditioning, the CS and US are separated by a stimulus-free interval. Traditional models suggest that a "handshake" between the CS and temporally delayed US is achieved by extending the duration of sensation-evoked activity throughout the trace period (Figure 8C). Here we report that A1 plasticity with trace conditioning required cholinergic inputs but was not accompanied by persistent activity throughout the trace period (Figures 3 and 4). Optogenetically tagged units in the caudal tail of the basal forebrain respond to aversive stimuli but also show short latency responses to tones (Figures 5 and 8D). At the start of trace conditioning, CS+-evoked spike rates were scaled up in basal forebrain neurons, and we observed a sharp increase in their functional coupling with the A1, as evidenced by increased spike-triggered CSD amplitude and increased gamma-band LFP coherence (Figures 6 and 8E). When conditioning was extended over many days, cholinergic basal forebrain neurons progressively increased their response to the CS+ frequency, ultimately filling in the 5-s trace period separating the CS and US (Figures 7 and 8F).

These findings support the general model for cortical plasticity arising from the convergent arrival of phasic ACh inputs and afferent sensory responses while challenging the specific assumptions that phasic cholinergic inputs from the basal forebrain are elicited only by the US and are invariant during learning. Taken together, our data demonstrate that electrophysiological signatures of brief sounds disappear within ~500 ms of stimulus offset in the ACx but that distributed forebrain circuits can bridge a CS-US gap ten times this long to support associative plasticity and learning. We cannot rule out that the sensory trace was maintained in the A1 during the 5-s silent gap through an intracellular signaling cascade, although this seems unlikely because a covert persistent sensory trace would have been reinforced by the delayed ACh pairing experiment (Figures 1F and 1G), in agreement with earlier findings (Metherate and Ashe, 1991).

Our data identify several stages of physiological changes that accompany auditory trace learning. During an initial stage, the novelty of sounds followed by aversive air puffs is accompanied by a temporally non-specific increase in the strength of functional coupling between the basal forebrain and the auditory cortex. This increase is fast, reaching its peak within the first 10 CS-US pairings (Figure 6J). Within tens of minutes following the start of conditioning, we observed enhanced CS+-evoked firing rates in ChACx units and A1 RSUs. Increased responses to the CS+ frequency in the A1 might be attributed to stronger CS+-evoked ACh release, but the plasticity within the basal forebrain itself is most readily explained by disinhibition or increased

tone-evoked excitatory inputs from an outside source, most likely the lateral amygdala or medial regions of the auditory thalamus, both of which show rapid changes in CS+-evoked firing rates and project to the caudal basal forebrain (Chavez and Zaborszky, 2017; Edeline and Weinberger, 1992; Hoffmann et al., 2018; Quirk et al., 1995; Weinberger, 2011). The lateral amygdala also coordinates increased synchrony with the prefrontal cortex and anterior cingulate cortex, which develops rapidly with CS+ conditioning and persist through the inter-trial interval, as we observed here (Likhtik et al., 2014; Taub et al., 2018a, 2018b). Following completion of the last conditioning block, CS+-specific receptive field remodeling was rapidly extinguished in the cholinergic basal forebrain (Figure 6B) but persisted in the cortex, consistent with observations that rapid plasticity in the cholinergic basal forebrain is involved in the induction but not maintenance of learned associations between sounds and reinforcers (Chubykin et al., 2013). Transient associative plasticity is also observed in lateral amygdala firing rates (Quirk et al., 1997) and amygdala-prefrontal theta coherence (Taub et al., 2018b), again suggesting that inputs from the lateral amygdala or its upstream input from the medial auditory thalamus may coordinate the time course of associative plasticity in the basal forebrain. On the other hand, the basolateral amygdala is also a primary target of cholinergic basal forebrain projections (Do et al., 2016). Disambiguating the chronology of changes in these interconnected brain areas could be addressed by simultaneous recordings from the amygdala and cholinergic basal forebrain neurons during auditory fear learning.

When auditory trace conditioning was extended over many days, we observed an over-representation of the CS+ frequency in cortical tonotopic maps that persisted even under anesthesia (Figure 2C) and enhanced responses to the CS+ in the cholinergic basal forebrain that extended beyond the CS period and into the trace period (Figures 7E and 7F). Although single-unit recordings identified stimulus-specific changes in basal forebrain spiking that began within minutes of pairing CS+ sounds with delayed air puffs (Figure 6B), sensation-evoked changes in the basal forebrain were slower to develop in our fiber photometry experiments. Different rates of associative plasticity could reflect a difference in sensitivity between single pixel bulk calcium imaging and single unit spiking, a difference in recording from all cholinergic neurons versus optogenetically identified ChACx neurons, or, alternatively, might indicate that associative learning is slower to develop when CSc and CS+ trials are interleaved during conditioning. These possibilities could be disambiguated by cellular-scale calcium imaging of basal forebrain cholinergic cell bodies combined with retrograde labeling to mark the subset of ChACx projection neurons.

Neocortical circuits feature highly conserved motifs of principal neurons, inhibitory interneurons, and long-range neuromodulatory inputs (Harris and Shepherd, 2015; Kepecs and Fishell, 2014). Sensory tuning properties of adult principal neurons can be rapidly scaled, shifted, or re-shaped in myriad configurations, depending on the complement of interneurons that is engaged by neuromodulatory inputs (Hangya et al., 2014; Kuchibhotla et al., 2017). Recent findings demonstrate that neuromodulatory inputs themselves are plastic and not accurately modeled as simple permissive gating factors. For example, basal forebrain cholinergic inputs to the ACx are strongly activated by reward as well as punishment, but the strength of the response is scaled by expectation (Hangya et al., 2015). Similarly, noradrenergic neurons in the *locus coeruleus* respond to painful stimuli such as a toe pinch but will rapidly scale up their responses to auditory stimuli that reliably precede the toe pinch (Martins and Froemke, 2015). Here we found that cholinergic neurons in the caudal tail of the basal forebrain change the magnitude and timing of their responses to auditory stimuli based on learned associations with delayed reinforcement. The combination of behaviorally regulated changes in neuromodulator timing and amplitude, combined with the substantial diversity of downstream local interneuron circuits, would further expand the degrees of freedom for modulating the response properties of cortical sensory neurons.

STAR★METHODS

Detailed methods are provided in the online version of this paper and include the following:

- KEY RESOURCES TABLE
- LEAD CONTACT AND MATERIALS AVAILABILITY
- EXPERIMENTAL MODEL AND SUBJECT DETAILS
- METHOD DETAILS
  - Preparation for awake head-fixed recordings
  - Single unit recordings in head-fixed mice
  - Analysis of LFP and CSD data
  - Antidromic tagging of cholinergic neurons
  - Head-fixed conditioning
  - Pharmacology experiments
  - Anesthetized extracellular cortical mapping
  - Auditory fear conditioning– freely moving mice
  - Cholinergic photometry during fear conditioning
  - Retrograde labeling of A1 projection neurons
- QUANTIFICATION AND STATISTICAL ANALYSIS
- DATA AND CODE AVAILABILITY

SUPPLEMENTAL INFORMATION

Supplemental Information can be found online at https://doi.org/10.1016/j.neuron.2019.06.024.

ACKNOWLEDGMENTS

We thank K. Hancock for developing data collection software. We thank R. Metherate for advice regarding pharmacology experiments and T. Hackett for assistance with initial anatomy experiments. We thank I. Carcea and A. Takesian for critical feedback on the manuscript. This work was supported by NIH Grant DC009836 (to D.B.P.), a Herchel Smith fellowship (to B.R.), and an HHMI international student fellowship (to W.G.).

AUTHOR CONTRIBUTIONS

W.G., B.R., and D.B.P. designed the experiments. W.G. and B.R. collected and analyzed the data with supervisory input from D.B.P. D.B.P. prepared the manuscript

DECLARATION OF INTERESTS

The authors declare no competing interests.

Received: August 29, 2018
Revised: May 24, 2019
Accepted: June 25, 2019
Published: July 24, 2019

REFERENCES

Aizenberg, M., Mwilambwe-Tshilobo, L., Briguglio, J.J., Natan, R.G., and Geffen, M.N. (2015). Bidirectional regulation of innate and learned behaviors that rely on frequency discrimination by cortical inhibitory neurons. PLoS Biol. *13*, e1002308.

Bakin, J.S., and Weinberger, N.M. (1990). Classical conditioning induces CS-specific receptive field plasticity in the auditory cortex of the guinea pig. Brain Res. *536*, 271–286.

Bakin, J.S., and Weinberger, N.M. (1996). Induction of a physiological memory in the cerebral cortex by stimulation of the nucleus basalis. Proc. Natl. Acad. Sci. USA *93*, 11219–11224.

Bauer, E.P., Paz, R., and Paré, D. (2007). Gamma oscillations coordinate amygdalo-rhinal interactions during learning. J. Neurosci. *27*, 9369–9379.

Blake, D.T., Heiser, M.A., Caywood, M., and Merzenich, M.M. (2006). Experience-dependent adult cortical plasticity requires cognitive association between sensation and reward. Neuron *52*, 371–381.

Buzsáki, G., and Schomburg, E.W. (2015). What does gamma coherence tell us about inter-regional neural communication? Nat. Neurosci. *18*, 484–489.

Buzsáki, G., and Wang, X.-J. (2012). Mechanisms of gamma oscillations. Annu. Rev. Neurosci. *35*, 203–225.

Chavez, C., and Zaborszky, L. (2017). Basal forebrain cholinergic-auditory cortical network: primary versus nonprimary auditory cortical areas. Cereb. Cortex *27*, 2335–2347.

Chernyshev, B.V., and Weinberger, N.M. (1998). Acoustic frequency tuning of neurons in the basal forebrain of the waking guinea pig. Brain Res. *793*, 79–94.

Chowdhury, N., Quinn, J.J., and Fanselow, M.S. (2005). Dorsal hippocampus involvement in trace fear conditioning with long, but not short, trace intervals in mice. Behav. Neurosci. *119*, 1396–1402.

Chubykin, A.A., Roach, E.B., Bear, M.F., and Shuler, M.G.H. (2013). A cholinergic mechanism for reward timing within primary visual cortex. Neuron *77*, 723–735.

Davis, M., Schlesinger, L.S., and Sorenson, C.A. (1989). Temporal specificity of fear conditioning: effects of different conditioned stimulus-unconditioned stimulus intervals on the fear-potentiated startle effect. J. Exp. Psychol. Anim. Behav. Process. *15*, 295–310.

Do, J.P., Xu, M., Lee, S.H., Chang, W.C., Zhang, S., Chung, S., Yung, T.J., Fan, J.L., Miyamichi, K., Luo, L., et al. (2016). Cell type-specific long-range connections of basal forebrain circuit. eLife *5*, 1–17.

Eckenstein, F., and Baughman, R.W. (1984). Two types of cholinergic innervation in cortex, one co-localized with vasoactive intestinal polypeptide. Nature *309*, 153–155.

Edeline, J.M., and Weinberger, N.M. (1992). Associative retuning in the thalamic source of input to the amygdala and auditory cortex: receptive field plasticity in the medial division of the medial geniculate body. Behav. Neurosci. *106*, 81–105.

Fries, P. (2015). Rhythms for cognition: communication through coherence. Neuron *88*, 220–235.

Froemke, R.C., Merzenich, M.M., and Schreiner, C.E. (2007). A synaptic memory trace for cortical receptive field plasticity. Nature *450*, 425–429.

Froemke, R.C., Carcea, I., Barker, A.J., Yuan, K., Seybold, B.A., Martins, A.R.O., Zaika, N., Bernstein, H., Wachs, M., Levis, P.A., et al. (2013). Long-term modification of cortical synapses improves sensory perception. Nat. Neurosci. *16*, 79–88.

Garcia, J., Ervin, F.R., and Koelling, R.A. (1966). Learning with prolonged delay of reinforcement. Psychon. Sci. *5*, 121–122.

Gilmartin, M.R., and McEchron, M.D. (2005). Single neurons in the medial prefrontal cortex of the rat exhibit tonic and phasic coding during trace fear conditioning. Behav. Neurosci. *119*, 1496–1510.

Hackett, T.A., Barkat, T.R., O'Brien, B.M.J., Hensch, T.K., and Polley, D.B. (2011). Linking topography to tonotopy in the mouse auditory thalamocortical circuit. J. Neurosci. *31*, 2983–2995.

Han, C.J., O'Tuathaigh, C.M., van Trigt, L., Quinn, J.J., Fanselow, M.S., Mongeau, R., Koch, C., and Anderson, D.J. (2003). Trace but not delay fear conditioning requires attention and the anterior cingulate cortex. Proc. Natl. Acad. Sci. USA *100*, 13087–13092.

Hangya, B., Pi, H.-J., Kvitsiani, D., Ranade, S.P., and Kepecs, A. (2014). From circuit motifs to computations: mapping the behavioral repertoire of cortical interneurons. Curr. Opin. Neurobiol. *26*, 117–124.

Hangya, B., Ranade, S.P., Lorenc, M., and Kepecs, A. (2015). Central cholinergic neurons are rapidly recruited by reinforcement feedback. Cell *162*, 1155–1168.

Harris, K.D., and Shepherd, G.M.G. (2015). The neocortical circuit: themes and variations. Nat. Neurosci. *18*, 170–181.

Harrison, T.C., Pinto, L., Brock, J.R., and Dan, Y. (2016). Calcium imaging of basal forebrain activity during innate and learned behaviors. Front. Neural Circuits *10*, 36.

Hoffmann, L.C., Zara, S.J., DeLord, E.D., and Mauk, M.D. (2018). Medial auditory thalamus Is necessary for expression of auditory trace eyelid conditioning. J. Neurosci. *38*, 8831–8844.

Janak, P.H., and Tye, K.M. (2015). From circuits to behaviour in the amygdala. Nature *517*, 284–292.

Kepecs, A., and Fishell, G. (2014). Interneuron cell types are fit to function. Nature *505*, 318–326.

Kilgard, M.P., and Merzenich, M.M. (1998). Cortical map reorganization enabled by nucleus basalis activity. Science *279*, 1714–1718.

Kim, J.-H., Jung, A.H., Jeong, D., Choi, I., Kim, K., Shin, S., Kim, S.J., and Lee, S.-H. (2016). Selectivity of neuromodulatory projections from the basal forebrain and locus ceruleus to primary sensory cortices. J. Neurosci. *36*, 5314–5327.

Kuchibhotla, K.V., Gill, J.V., Lindsay, G.W., Papadoyannis, E.S., Field, R.E., Sten, T.A.H., Miller, K.D., and Froemke, R.C. (2017). Parallel processing by cortical inhibition enables context-dependent behavior. Nat. Neurosci. *20*, 62–71.

Lerner, T.N., Shilyansky, C., Davidson, T.J., Evans, K.E., Beier, K.T., Zalocusky, K.A., Crow, A.K., Malenka, R.C., Luo, L., Tomer, R., and Deisseroth, K. (2015). Intact-brain analyses reveal distinct information carried by SNc dopamine subcircuits. Cell *162*, 635–647.

Letzkus, J.J., Wolff, S.B.E., Meyer, E.M.M., Tovote, P., Courtin, J., Herry, C., and Lüthi, A. (2011). A disinhibitory microcircuit for associative fear learning in the auditory cortex. Nature *480*, 331–335.

Letzkus, J.J., Wolff, S.B.E., and Lüthi, A. (2015). Disinhibition, a circuit mechanism for associative learning and memory. Neuron *88*, 264–276.

Likhtik, E., Stujenske, J.M., Topiwala, M.A., Harris, A.Z., and Gordon, J.A. (2014). Prefrontal entrainment of amygdala activity signals safety in learned fear and innate anxiety. Nat. Neurosci. *17*, 106–113.

Lin, S.-C.C., and Nicolelis, M.A.L. (2008). Neuronal ensemble bursting in the basal forebrain encodes salience irrespective of valence. Neuron *59*, 138–149.

Ma, X., and Suga, N. (2003). Augmentation of plasticity of the central auditory system by the basal forebrain and/or somatosensory cortex. J. Neurophysiol. *89*, 90–103.

Maho, C., Hars, B., Edeline, J.M., and Hennevin, E. (1995). Conditioned changes in the basal forebrain: Relations with learning-induced cortical plasticity. Psychobiology *23*, 10–25.

Martins, A.R.O., and Froemke, R.C. (2015). Coordinated forms of noradrenergic plasticity in the locus coeruleus and primary auditory cortex. Nat. Neurosci. *18*, 1483–1492.

McGann, J.P. (2015). Associative learning and sensory neuroplasticity: how does it happen and what is it good for? Learn. Mem. *22*, 567–576.

Metherate, R., and Ashe, J.H. (1991). Basal forebrain stimulation modifies auditory cortex responsiveness by an action at muscarinic receptors. Brain Res. *559*, 163–167.

Miltner, W.H.R., Braun, C., Arnold, M., Witte, H., and Taub, E. (1999). Coherence of gamma-band EEG activity as a basis for associative learning. Nature *397*, 434–436.

Nelson, A., and Mooney, R. (2016). The basal forebrain and motor cortex provide convergent yet distinct movement-related inputs to the auditory cortex. Neuron *90*, 635–648.

Pavlov, I.P. (1932). The reply of a physiologist to psychologists. Psychol. Rev. *39*, 91–127.

Pi, H.J., Hangya, B., Kvitsiani, D., Sanders, J.I., Huang, Z.J., and Kepecs, A. (2013). Cortical interneurons that specialize in disinhibitory control. Nature *503*, 521–524.

Plakke, B., Freeman, J.H., and Poremba, A. (2009). Metabolic mapping of rat forebrain and midbrain during delay and trace eyeblink conditioning. Neurobiol. Learn. Mem. *92*, 335–344.

Quirk, G.J., Repa, C., and LeDoux, J.E. (1995). Fear conditioning enhances short-latency auditory responses of lateral amygdala neurons: parallel recordings in the freely behaving rat. Neuron *15*, 1029–1039.

Quirk, G.J., Armony, J.L., and LeDoux, J.E. (1997). Fear conditioning enhances different temporal components of tone-evoked spike trains in auditory cortex and lateral amygdala. Neuron *19*, 613–624.

Raybuck, J.D., and Lattal, K.M. (2014). Bridging the interval: theory and neurobiology of trace conditioning. Behav. Processes *101*, 103–111.

Reed, A., Riley, J., Carraway, R., Carrasco, A., Perez, C., Jakkamsetti, V., and Kilgard, M.P. (2011). Cortical map plasticity improves learning but is not necessary for improved performance. Neuron *70*, 121–131.

Siegel, J.J., Kalmbach, B., Chitwood, R.A., and Mauk, M.D. (2012). Persistent activity in a cortical-to-subcortical circuit: bridging the temporal gap in trace eyelid conditioning. J. Neurophysiol. *107*, 50–64.

Takesian, A.E., Bogart, L.J., Lichtman, J.W., and Hensch, T.K. (2018). Inhibitory circuit gating of auditory critical-period plasticity. Nat. Neurosci. *21*, 1.

Taub, A.H., Shohat, Y., and Paz, R. (2018a). Long time-scales in primate amygdala neurons support aversive learning. Nat. Commun. *9*, 4460.

Taub, A.H., Perets, R., Kahana, E., and Paz, R. (2018b). Oscillations synchronize amygdala-to-prefrontal primate circuits during aversive learning. Neuron *97*, 291–298.e3.

Urban-Ciecko, J., Jouhanneau, J.S., Myal, S.E., Poulet, J.F.A., and Barth, A.L. (2018). Precisely timed nicotinic activation drives SST inhibition in neocortical circuits. Neuron *97*, 611–625.e5.

Weinberger, N.M. (2011). The medial geniculate, not the amygdala, as the root of auditory fear conditioning. Hear. Res. *274*, 61–74.

Williamson, R.S., and Polley, D.B. (2019). Parallel pathways for sound processing and functional connectivity among layer 5 and 6 auditory corticofugal neurons. eLife *8*, e42974.

Zhang, G.W., Sun, W.J., Zingg, B., Shen, L., He, J., Xiong, Y., Tao, H.W., and Zhang, L.I. (2018). A non-canonical reticular-limbic central auditory pathway via medial septum contributes to fear conditioning. Neuron *97*, 406–417.e4.

STAR★METHODS

KEY RESOURCES TABLE

REAGENT or RESOURCE	SOURCE	IDENTIFIER
Chemicals, Peptides, and Recombinant Proteins		
Ketamine hydrochloride	Vedco	Cat#NDC 50989-161-06
Xylazine	Bayer Animal Health	Cat#CAS 7361-61-7
Lidocaine hydrochloride	Hospira Inc.	Cat# 71-157-DK
Buprenorphine hydrochloride	Buprenex	Cat#NDC 12496-0757-5
Red retrobeads	LumaFluor	Cat#Red Retrobeads IX (100 ml)
Isoflurane	Piramal	Cat#NDC 66794-013-10
Flow-It ALC Flowable Composite	Pentron	Cat#N11B
Methyllycaconitine Citrate Salt	Sigma-Aldrich	Cat#M168-25MG
Atropine Sulfate	Sigma-Aldrich	Cat#1045009-500MG
Dihydro-b-erythroidine hydrobromide	Tocris	Cat#2349/10
C&B Metabond Quick Adhesive Cement System	Parkell	Cat#S380
VECTASHIELD HardSet Antifade Mounting Medium with DAPI	VectorLabs	Cat#H-1500
Silicon adhesive	WPI	Cat#KWIK-SIL
Experimental Models: Organisms/Strains		
Mouse: Ai32: B6;129S-Gt(ROSA)26Sortm32(CAG-COP4*H134R/EYFP)Hze/J	The Jackson Laboratory	RRID:IMSR_JAX:012569
Mouse: Ai148D: B6.Cg-Igs7tm148.1(tetO-GCaMP6f, CAG-tTA2)Hze/J	The Jackson Laboratory	RRID:IMSR_JAX:030328
Mouse: Chat-Cre: B6;129S6-Chattm2(cre)Lowl/J	The Jackson Laboratory	RRID:IMSR_JAX:006410
Software and Algorithms		
Labview 2015	National Instruments	https://www.ni.com/en-us/shop/labview.html
OpenEx Software Suite	Tucker-Davis Technologies	https://www.tdt.com/component/openex-software-suite/
Wave_clus	https://doi.org/10.1152/jn.00339.2018	https://github.com/csn-le/wave_clus
MATLAB 2013b	Mathworks	https://www.mathworks.com/products/matlab.html
Other		
Linear silicone recording electrode	NeuroNexus	NeuroNexus A1x16-100-177-3mm
Linear silicone recording electrode	NeuroNexus	NeuroNexus A1x16-50-177-5mm
Plate Clamps	Altechna	Cat#4PC69
Diode laser (473 nm)	Omicron	LuxX_ 473-100
BioAmp processor	Tucker-Davis Technologies	RZ5D
Free-field Electrostatic speaker	Tucker-Davis Technologies	ES1
PXI Controller	National Instruments	PXIe-8840
Connectorized LED, Violet 405	Doric	CLED_405
Connectorized LED, Blue 465	Doric	CLED_465
LED driver	Doric	LEDD_2
Fluorescence minicube	Doric	FMC4_AE(405)_E(460-490)_F(500-550)_S
Newport photoreceiver	Doric	NPM_2151_FOA_FC
Branching fiberoptic patchcord	Doric	BFP(2)_300/330/LWMJ-0.37_1m_FCM*-2xFC
Rotary joint	Doric	AHRJ-OE_PT_AH_12_USB-C
Mono fiberoptic patchcord	Doric	MFP_960/1000/2200-0.63_0.5m_FC-FC

(*Continued on next page*)

Continued

REAGENT or RESOURCE	SOURCE	IDENTIFIER
Fiberoptic patchcable	Doric	MFP_400/460/900-0.48_0.54m_FC-ZF1.25
Mono fiberoptic cannula	Doric	MFC_400/430-0.48_5.5mm_MF1.25_FLT
Bronze sleeve	Doric	SLEEVE_BR_1.25

LEAD CONTACT AND MATERIALS AVAILABILITY

Further information and requests for resources and reagents should be directed to and will be fulfilled by the Lead Contact, Daniel Polley (daniel_polley@meei.harvard.edu). This study did not generate new unique reagents.

EXPERIMENTAL MODEL AND SUBJECT DETAILS

All procedures were approved by the Massachusetts Eye and Ear Infirmary Animal Care and Use Committee and followed the guidelines established by the National Institutes of Health for the care and use of laboratory animals. For studies of trace conditioning and cortical map plasticity, 8 adult CBA/CaJ mice of either sex were used. For head-fixed recording experiments, 35 adult ChAT-IRES-Cre × Ai32 transgenic mice of either sex were used (Jackson Labs stock numbers 006410 and 012569, respectively). For retrograde labeling experiments, 5 adult ChAT-IRES-Cre × Ai32 transgenic mice of either sex were used. For basal forebrain fiber photometry experiments, 9 adult ChAT-IRES-Cre × Ai148 transgenic mice of either sex were used (Jackson Labs stock numbers 006410 and 030328 respectively). Mice that had undergone a major survival surgery were housed individually. Otherwise, mice were group housed. Mice were maintained in a 12/12 light/dark cycle with food and water available *ad libitum*.

METHOD DETAILS

Preparation for awake head-fixed recordings

Mice were brought to a surgical plane of anesthesia with ketamine/xylazine (induction with 100 mg/kg ketamine and 10 mg/kg xylazine, with 50–60 mg/kg ketamine supplements as necessary). Lidocaine hydrochloride was injected subcutaneously to numb the surgical site. Body temperature was maintained at 36.5° with a homeothermic blanket system (Fine Science Tools). The periosteum overlying the dorsal surface of the skull was completely removed. The skull surface was prepared with 70% ethanol and etchant (C&B Metabond). A custom titanium head plate was then cemented to the skull, centered on Bregma. After recovery, animals were housed individually. Animals were given at least 48 hours to acclimate to the head plate before any further experiments.

On the day of the first recording session, animals were briefly anesthetized with isoflurane (1.5% in oxygen) while a small craniotomy (0.5 × 1.0 mm, medial-lateral × rostral-caudal) was made along the caudal end of the right temporal ridge, 1mm rostral to the lambdoid suture to expose A1. A second craniotomy (1.0 × 1.0 mm, medial-lateral × rostral-caudal) was centered at 2.5 mm lateral and 1.5 mm caudal to bregma also in the right cortex to access the basal forebrain. Small chambers were built around the craniotomies with UV-cured cement and filled with lubricating ointment (Paralub Vet Ointment). At the end of each recording session, the chamber was flushed, filled with fresh ointment, and capped with UV-cured cement (Flow-It ALC).

Single unit recordings in head-fixed mice

On the day of recording, the head of the animal was immobilized by attaching the head plate to a rigid clamp (Altechna). Mice could walk freely on a disk that was mounted atop a low-friction silent rotor and a high-sensitivity optical rotary encoder. Continuous monitoring of the eye and disk rotation confirmed that all recordings were made in the awake condition. Recordings were performed inside a dimly lighted single-wall sound attenuating chamber (Acoustic Systems). For A1 columnar recordings, a single-shank linear silicon probe (NeuroNexus A1x16-100-177-3mm) was inserted into the auditory cortex perpendicular to the brain surface using a 3-D micromanipulator (Narishige) and a hydraulic microdrive (FHC) with the tip of the probe positioned approximately 1.3 mm below the cortical surface, such that the top 2 electrode contacts were outside the brain, the bottom 2 contacts were in the white matter or hippocampus, and the middle 11-12 contacts spanned all six layers of the auditory cortex. At the beginning of the first recording session, several penetrations were made along the caudal-rostral extent of the craniotomy to locate the high-frequency reversal of the tonotopic gradient that demarcates the rostral boundary of mouse A1 (Hackett et al., 2011). For basal forebrain recordings, a second silicon probe (NeuroNexus A1X16-50-177-5mm) was inserted into the other craniotomy with the depth of the probe tip around 3.8 - 4.3 mm below the pial surface.

Digital waveforms for the laser command signal and acoustic stimuli were generated with a 24-bit digital-to-analog converter (PXI, National Instruments) using custom MATLAB (MathWorks) and LabVIEW (National Instruments) scripts. Acoustic stimuli were presented via a freefield electrostatic speaker positioned 10cm from the left ear canal (Tucker-Davis Technologies). Stimuli were calibrated using a wide-band ultrasonic acoustic sensor (Knowles Acoustics, model SPM0204UD5). Laminar location of A1 recording sites were determined from the laminar current source density (CSD), evoked by broadband noise bursts (50 ms duration, 4 ms

onset/offset cosine ramps, 1 s inter-stimulus interval [ISI], 70 dB SPL, 50 repetitions). Frequency-rate functions were derived from responses to pure tone pips (250 ms duration, 4 ms onset/offset cosine ramps, 1 s ISI, 4-45 kHz with 0.25 octave steps, 70 dB SPL, 15 repetitions of each stimulus, pseudo-randomized). Frequency response areas (FRAs) were also measured using pure tone stimuli (250 ms duration, 4ms onset/offset cosine ramps, 1 s, ISI, 4 – 64 kHz with 0.1 octave steps, 0 – 70 dB SPL with 10 dB steps, 2 repetitions of each stimulus, pseudo-randomized).

Raw neural signals were digitized at 32-bit, 24.4 kHz and stored in binary format (Neurodigitizer and RZ5 BioAmp Processor; Tucker-Davis Technologies). To eliminate artifacts, the common mode signal (channel-averaged neural traces) was subtracted from all channels in the brain. In experiments where simultaneous recordings were made from probes in A1 and basal forebrain, the common mode removal was performed independently for each probe. Electrical signals were notch filtered at 60Hz, then band-pass filtered (300-3000 Hz, second order Butterworth filters), from which the multiunit activity was extracted as negative deflections in the electrical trace with an amplitude exceeding 4 s.d. of the baseline hash. Single units were separated from multiunit activity using a wavelet-based spike sorting package (wave_clus). Single unit isolation was confirmed based on the inter-spike-interval histogram (less than 3% of the spikes in the 0-3 ms bins) and the consistency of the spike waveform (s.d of peak-to-trough delay of spikes within the cluster less than 200 μs). The average trough-to-peak delay from each single unit formed a bi-modal distribution, allowing us to separate regular-spiking putative pyramidal neuron waveforms (> 0.4 ms) from fast-spiking waveforms (< 0.4 ms) (Figure 1B).

Analysis of LFP and CSD data

To extract local field potentials (LFP), raw signals were notch filtered at 60 Hz and down-sampled to 1000 Hz. The CSD was calculated as the second spatial derivative of the LFP signal. To eliminate potential artifacts introduced by impedance mismatching between channels, signals were spatially smoothed along the channels with a triangle filter (5-point Hanning window). Noise-evoked columnar CSD patterns were used to determine the location of the A1 recording channel. Two CSD signatures were used to identify L4: A brief current sink first occurs approximately 10 ms after the noise onset, which was used to determine the lower border of L4 (white arrow, Figure 1B). A tri-phasic CSD pattern (sink-source-sink from upper to lower channels) occurs between 20 ms and 50 ms, where the border between the upper sink and the source was used to define the upper boundary of L4.

Spike-triggered CSD amplitude and gamma coherence were measured from dual recordings of the basal forebrain and auditory cortex during conditioning blocks. CSD amplitude from an electrode assigned to each layer was calculated relative to spontaneously occurring basal forebrain spikes recorded during a 25-30 s window at the end of each trial (Figure 6D). The peak to trough difference of the spike-triggered averaged CSD waveform was used to define the response amplitude. Magnitude-squared coherence estimate (mscohere in MATLAB) was used to analyze the coherence between LFPs measured simultaneously from A1 and the basal forebrain. The basal forebrain LFP was computed as the averaged signal across all electrodes. LFPs from A1 electrodes spanning L1 to L6 were treated separately with individual coherence calculated with the reference basal forebrain LFP. Four sets of coherence measurements were calculated with data from four 1 s duration windows during each conditioning trial: *i)* 0-1 s following CS onset (CS epoch); *ii)* 3-4 s after sound offset (trace epoch); *iii)* 0-1 s after US onset (US epoch) and *iv*) from 39-40 s after CS onset (spontaneous epoch). Coherence measurements were averaged over the 10 trials in each of six conditioning blocks. The gamma-band coherence was defined as the averaged magnitude-squared coherence between 40 to 80 Hz.

Antidromic tagging of cholinergic neurons

To identify ChAT+ neurons in the basal forebrain that project to the auditory cortex (ChACx), brief laser pulses were delivered to the surface of the exposed auditory cortex with a diode laser coupled to an optic fiber (LuxX, Omicron; 473 nm, 50 ms duration, 2.55 mW/mm^2, 1 s inter-trial intervals, 50 trials). Unit responses from basal forebrain recording sites were analyzed as peri-stimulus time histograms (PSTHs). According to the response profile, three types of units were identified: direct antidromically activated units which exhibited short latency (5 – 15 ms) and low inter-trial jitter (< 2 ms); indirect antidromically activated units which exhibited long latency (typically 30 – 60 ms) and high inter-trial jitter (> 2 ms); and non-antidromically activated units which did not show significant responses to laser. Laser responses were monitored periodically during the experiment and only units with consistent response profiles were analyzed.

Head-fixed conditioning

Pairing sound with air puffs

Mice were acclimated to head-fixation for at least an hour before conditioning began. Pressurized air puffs (0.5 s duration) were delivered via a nozzle made of flexible tubing (1.2cm inner diameter) positioned 1cm from the muzzle. The nozzle could be directed at the muzzle or away from the muzzle. In CS+ trials, an air puff was delivered 5 s after the offset of a NBN burst (4th order Butterworth band-pass filter, 0.25 octave bandwidth, 2 s duration with 5 ms cosine ramp at stimulus onset and offset, 70 dB SPL). In CS-control trials, no air puff was delivered. To control for the sound of the air puff without the aversive, tactile stimulation, the nozzle was directed away from the muzzle. The center frequency of the NBN conditioning stimulus was manually set by evaluating frequency tuning functions on each responsive electrode and selecting a center frequency that was at least 0.5 octaves away from the best frequency of all recording sites.

Pairing sound with cholinergic terminal stimulation

Cholinergic neurons were optogenetically activated by shining blue light onto the exposed brain surface (473 nm, 2 s duration, 2.55 mW/mm^2) with a diode laser coupled to an optic fiber (LuxX, Omicron). The fiber tip was positioned approximately 1cm above the exposed surface of A1. Two versions of ACh pairing protocols were used: a delayed ACh photoactivation, where laser onset occurred 5 s after NBN offset, and a simultaneous photoactivation experiment where the ACh photoactivation overlapped with the NBN presentation.

Neurophysiology data analysis

Frequency response functions were measured at least twice before the first conditioning block, six times in between each conditioning blocks, and at least 4 times after the last conditioning block. Each of the six conditioning blocks consisted of 10 trials (40 s duration each, Figures 1C and 6D). CS-specific changes in firing rate were quantified by first normalizing the response between the values 0 and 1, such that a value of 1.0 equaled the response at the best frequency. We then computed the average fold-change in normalized response at frequencies far away from the paired/conditioning frequency ($> \pm 0.25$ octaves, blue shaded region in Figure 1E) and subtracted this value from the average fold-change in spiking at or near the paired/conditioning frequency (≤ 0.25 octaves, red). The resultant Plasticity Index is a marker of associative plasticity, where values greater than 0 indicate disproportionately enhanced spiking at the CS frequency and/or reduced spiking away from the CS frequency.

Analysis of freezing behavior

To quantify head-fixed freezing behavior, the rotary wheel encoder signal was downsampled to 1 kHz and smoothed with a 100-point Hanning window using a zero phase lag digital filter. Movement velocity was calculated as the first derivative of the wheel position signal. Freezing was operationally defined for individual time samples during conditioning blocks as a zero-velocity signal. We computed the percentage change in the fraction of time samples with freezing behavior between a 5 s time epoch immediately prior to CS onset relative to a 1 s time window occurring 3-4 s after CS offset (i.e., during the trace period for CS+ conditioning blocks). The percentage change in freezing was averaged across all single trials within the session.

Pharmacology experiments

To block A1 cholinergic synapses shortly before neurophysiological recordings, 100 nL of solution was injected into ACtx 500 μm below the brain surface at a speed of 10 nl/min using a motorized injector (Stoelting Co.). The solution contained 10 μM of atropine sulfate, 1 μM of dihydro-b-erythroidine hydrobromide, and 150 μM methyllycaconitine citrate dissolved in artificial cerebrospinal fluid. For the control experiments, 100 nL of artificial cerebrospinal fluid was injected. The injection pipette was removed 5 minutes following the injection and the animal was transferred to the head-fixed recording rig. Recordings began once the mouse exhibited normal treadmill running and grooming behavior.

Anesthetized extracellular cortical mapping

Mice were brought to a surgical plane of anesthesia with ketamine/xylazine (induction with 100 mg/kg ketamine and 10 mg/kg xylazine, with 50–60 mg/kg ketamine supplements as necessary). Buprivicaine was injected subcutaneously to numb the surgical site. The core body temperature of the animal was maintained at 36.5°C with a homeothermic blanket system (Fine Science Tools). Using a scalpel, a 4 × 3mm (rostrocaudal × mediolateral) craniotomy was made in the right auditory cortex, approximately centered on a point 2.8 mm posterior and 4.4 mm lateral to bregma, and the dura mater was left intact. The brain surface was covered with high-viscosity silicon oil and photographed. Simultaneous recordings were made from the middle layers of the right auditory cortex (420–430 μm from pial surface) with 2–4 epoxylite-coated tungsten microelectrodes (FHC). The location of each recording site was manually marked on a high-resolution photograph of the brain surface.

Sound stimuli were generated with a 24-bit digital-to-analog converter (National Instruments model PXI-4461) delivered to the ear canal via acoustic assemblies consisting of two miniature dynamic earphones (CUI CDMG15008–03A) and an electret condenser microphone (Knowles FG-23339-PO7) coupled to a probe tube. Stimuli were calibrated at the tympanic membrane in each mouse before recording. Normal function of the auditory periphery and accurate placement of the probe tube in the ear canal were confirmed by monitoring the threshold and amplitude of cochlear distortion product otoacoustic emissions. Frequency response areas were measured with pseudorandomly presented tone pips (50 ms duration, 4 ms raised cosine onset/offset ramps, 0.5–1 s inter-trial interval) of variable frequency (4–64 kHz in 0.1 octave increments) and level (0–60 dB SPL in 5 dB increments). A total of 533 unique frequency-level combinations were presented once or twice for a given recording site. Recordings were performed inside a double-wall sound attenuating chamber (ETS-Lindgren).

Raw neural signals were digitized at 32-bit, 24.4 kHz (Digitizer and BioAmp Processor; Tucker-Davis Technologies) and stored in binary format. Subsequent analyses were performed in MATLAB (MathWorks). The signals were notch filtered at 60 Hz and then band-pass filtered at 400–3000 Hz with a second-order Butterworth filter. Multiunit spiking was detected as negative threshold-crossing events (-4.5 SDs from the mean). For each recording site, a FRA was constructed based on the onset portion of the tone-evoked spiking (10 – 40 ms), and the best frequency was assigned based on the highest firing rate. As described previously, A1 and AAF were identified based on the stereotypical low-to-high-to-low frequency tonotopic organization across the caudal-rostral axis (Hackett et al., 2011). Tonotopy was reconstructed from 40-60 approximately evenly spaced individual recording sites with a 0.5 × 1.5 mm (lateral-medial × rostral-caudal) strip spanning the center portion of the A1-AAF extent (Figure 2). The high-frequency mirror reversal boundary separating A1-AAF was used as a common anchor point to align maps from different mice.

Auditory fear conditioning– freely moving mice

Behavioral paradigm

Fear conditioning was performed inside an acoustically transparent enclosure (20 × 15 × 30 cm, L × W × H) resting atop electrified flooring (8 pole scrambled shocker, Coulbourn Instruments). The acoustic enclosure was maintained inside a double-wall sound attenuating chamber (ETS-Lindgren). Acoustic stimuli and foot shock trigger signals were generated on a National Instruments PXI system using custom software programmed in LabVIEW. Auditory stimuli were delivered through a calibrated electrostatic free-field speaker positioned above the apparatus (Tucker-Davis Technologies). Mice were given at least 5 min to acclimate to the apparatus before each conditioning session. The CS+ stimulus was a 2 s long NBN burst centered at 16 kHz. The CS-control stimulus was a NBN with 8 kHz as its center frequency. Each session consists of 6 alternating conditioning blocks between CS+ and CSc, with 10 trials in each block. During every CS+ trial, a foot shock (0.1 mA, 1 s duration) was delivered 5 s after the offset of the sound. Foot shocks were not delivered on CSc trials. Inter-trial intervals were randomly chosen between 30 s to 40 s. A passive exposure control group was presented with the same NBN stimuli without any foot shocks. Following five consecutive days of conditioning, mice were placed in a novel context on Day 6 and given at least 5 min to acclimate to the apparatus before the testing. On test sessions, 20 trials of randomized CS+ and CSc were delivered without foot shocks (inter-trials intervals randomized between 60-90 s).

Analysis of freezing behavior

Mouse movement were captured with a commercial webcam at 20 frames/s and processed online with custom movement analysis software (LabVIEW, National Instruments). After thresholding, a low spatial frequency blob detection was performed by iteratively eroding and dilating the image. Using only pixels that fell within the outline of the mouse, the previous grayscale frame was subtracted from the reference frame. Significant motion pixels were identified for each frame as pixels where values (8-bit) changed by more than 50 grayscale units. For each individual video frame, freezing was operationally defined as those containing fewer than 20 significant motion pixels. Percent time spent frozen was calculated for a 1 s period beginning 3 s after the CS offset.

Cholinergic photometry during fear conditioning

Behavior

Mice were conditioned over 7 consecutive days in a chamber (20 × 20 × 33 cm, L × W × H) positioned inside a single-wall sound-attenuating booth. Mice were given at least 5 minutes to acclimate to the chamber before each recording session. The visual and tactile sensory context inside the chamber was modified between baseline (D1), conditioning (D2-6) and testing (D7) by changing the wall and floor inserts. The CS+ stimulus was a 2 s long NBN burst centered at 5.9kHz. The CSc stimulus was a NBN with 11kHz as its center frequency. On training days, the presentation of the CS+ stimulus was paired with a foot shock (0.1mA, 1 s duration) delivered 5 s after the sound offset via an electrified floor grid (8 pole scrambled shocker, Coulbourn Instruments). During baseline (D1) and conditioning (D2-6), blocks of 10 CS+ and 10 CSc trials were alternately presented, to match the fear conditioning procedure described above. On the testing day (D7), we presented 20 pseudorandomly ordered CS+ and CSc trials (10 each). Inter-trial intervals were randomized between 30-40 s. Analysis of freezing behavior followed the description above.

Surgery for fiber photometry

Mice were anesthetized with 2% isoflurane and placed in a stereotaxic frame (Kopf Model 1900). The optical fiber implant (Doric, 400um core 0.48NA, 1.25mm diameter low-autofluorescence metal ferrule) was slowly lowered into the caudal basal forebrain (2.5 × −1.5 × 4.0 mm from bregma, [lateral × caudal × ventral]). The exposed cortex was protected with a silicon adhesive (WPI Kwik-Sil) and the implant was secured with dental cement (C&B Metabond). A titanium headplate was cemented on the skull. Mice recovered for at least 3 weeks before imaging began.

Fiber photometry data collection

LEDs of different wavelengths provided a basis for separating calcium-dependent (465 nm) and calcium-independent (405nm) fluorescence. Blue and purple LEDs were modulated at 211Hz and 531Hz, respectively, and combined through an integrated fluorescence mini-cube (FMC4, Doric). The excitation light was delivered to the implant through a patch cord connected to a rotary joint (AHRJ, Doric). The power at the tip of the patch cable was 0.1-0.2mW. The optical patch cable was connected to the fiber implant via a bronze mating sleeve. Bulk fluorescent signals were acquired with a femtowatt photoreceiver (2151, Newport) and digital signal processor (Tucker-Davis Technologies RZ5D). The signal was demodulated by the lock-in amplifier implemented in the processor, sampled at 1017Hz and low-pass filtered with a corner frequency at 20Hz.

Analysis of fiber photometry data

After demodulation, a least-square fit of the 405nm signal to the 465nm signal was calculated for each trial. Fractional change, $\Delta F/F$, was calculated as (465nm – 405nm_fitted)/405nm_fitted; (Lerner et al., 2015). CS+ and CSc trials on baseline and conditioning days were grouped into three blocks of 10 trials before averaging and calculating a $\Delta F/F$ trace for each block. Average $\Delta F/F$ were down-sampled at 20Hz. Each trial consisted of four response epochs: baseline (1 s window immediately prior to sound onset), CS (0.5 s starting at sound onset), trace (5 s window beginning at sound offset) and US (4 s window beginning at 5 s after sound offset). Response amplitude during each epoch was calculated for each block of 10 trials by summing all $\Delta F/F$ values above the mean $\Delta F/F$ value from the baseline epoch and then compensating for the variable duration of the CS, trace and US response periods. Response amplitudes were then averaged so that each mouse provided a single value for the CS, trace and US epochs of CS+ and CSc trials for each of the seven imaging days. To minimize variability between mice, response amplitude values were assigned

a z-score relative to the distribution of all 42 data points (7 days x 2 stimuli x 3 time epochs). Photometry signals from 4/9 mice were either unmeasurable or intractably contaminated by movement-related artifacts, leaving us with N = 5 mice that provided the complete set of imaging and behavioral data over a 7d period. A permutation test was used to compare the response scores of CS+ and CSc trials for each day and each epoch. A distribution of the means of the difference between the CS+ and CSc trials was calculated by randomly assigning the ''CS+'' and ''CSc'' identity in each pair of scores within a subject (100,000 repetitions).

Retrograde labeling of A1 projection neurons

ChAT-IRES-Cre × Ai32 transgenic mice (N = 4) were anesthetized with ketamine (100 mg/kg) and xylazine (10 mg/kg). A surgical plane of anesthesia was maintained throughout the procedure with supplements of ketamine (50 mg/kg) as needed. We then injected 0.3 μl of red retrobeads (LumaFluor Inc.) into A1 at 0.05 – 0.1 μl/min using a motorized injector (Stoelting Co.). After allowing 7 days for retrograde transport, mice were deeply anesthetized with ketamine and prepared for transcardial perfusion with a 4% formalin solution in 0.1M phosphate buffer. The brains were extracted and post-fixed at room temperature for an additional 12 hours before transfer to 30% sucrose solution. Coronal sections (30 μm thick) were prepared on a cryostat and counterstained with DAPI (VECTASHIELD HardSet Antifade Mounting Medium with DAPI). The location of the injection site in ACtx was confirmed in each case (Figure S4). All sections containing the basal forebrain were analyzed by counting the number of bead+ and ChAT+ cells. Bead+ cells were defined as distinct oval shapes with more than 10 bead pixels inside and a DAPI-stained nucleus in the middle. ChAT+ cells were identified based on the shape and the intensity of the EYFP signal.

QUANTIFICATION AND STATISTICAL ANALYSIS

All statistical analysis was performed with MATLAB (Mathworks). Descriptive statistics are reported as mean ± SEM unless otherwise indicated. In cases where the same data sample was used for multiple comparisons, we used the Holm-Bonferroni correction to adjust for the increased probability of Type-I error. Non-parametric statistical tests were used in select cases where data samples did not meet the assumptions of parametric statistical tests, as determined from the Lillefors test for normality. Statistical significance was defined as $p < 0.05$.

DATA AND CODE AVAILABILITY

The datasets and code supporting the current study have not been deposited in a public repository due to size but are available from the corresponding author on reasonable request at daniel_polley@meei.harvard.edu.